

# JGR Earth Surface

## RESEARCH ARTICLE

10.1029/2021JF006169

### Key Points:

- A centroid analysis and shoreline modeling identified the influence of the dune system on shoreline evolution over a range of time-scales
- Different beach migration modes (steepening/flattening and advance/retreat) were identified using a centroid analysis
- Our analysis showed that time-scales related to dune erosion and recovery play an important role in shoreline modeling performance

### Correspondence to:

J. Montaño,  
jmon177@aucklanduni.ac.nz

### Citation:

Montaño, J., Coco, G., Chataigner, T., Yates, M., Le Dantec, N., Suanez, S., et al. (2021). Time-scales of a dune-beach system and implications for shoreline modeling. *Journal of Geophysical Research: Earth Surface*, 126, e2021JF006169. <https://doi.org/10.1029/2021JF006169>

Received 18 MAR 2021  
Accepted 1 OCT 2021

## Time-Scales of a Dune-Beach System and Implications for Shoreline Modeling

Jennifer Montaño<sup>1</sup> , Giovanni Coco<sup>1</sup> , Teddy Chataigner<sup>2</sup>, Marissa Yates<sup>2</sup> , Nicolas Le Dantec<sup>3</sup>, Serge Suanez<sup>4</sup>, Laura Cagigal<sup>1</sup> , France Floc'h<sup>4</sup> , and Ian Townend<sup>5</sup> 

<sup>1</sup>School of Environment, Faculty of Science, University of Auckland, Auckland, New Zealand, <sup>2</sup>Saint-Venant Hydraulics Laboratory & Cerema, Chatou, Paris, France, <sup>3</sup>LGO UMR 6538 CNRS, IUEM, UBO & Cerema, Plouzané, France, <sup>4</sup>LETG UMR 6554 CNRS, UBO, Plouzané, France, <sup>5</sup>University of Southampton, Southampton, England

**Abstract** Understanding the interactions between dune systems and beaches is critical to determining the short-term shoreline response and the long-term resilience. In this study, almost 15 years of monthly beach/dune measurements were analyzed for three different profiles at Vougot Beach, France to understand and predict shoreline changes from intra-annual to multi-annual time-scales. Four migration modes: advance/retreat (translation modes) and steepening/flattening (rotation modes) were identified through a centroid analysis. The analysis showed that translation and rotation can occur simultaneously, with long-term trends of beach retreat and profile steepening (lower beach retreating and upper beach advancing), which was interrupted by two energetic wave events causing profile flattening (lower beach advancing and upper beach retreating). These two observations are evidence of how the sediment contribution resulting from the dune erosion events temporarily caused a large advance in the shoreline position. A recent modeling approach that accounts for different time-scales is applied to predict the shoreline changes, showing significant improvements in comparison to a traditional shoreline equilibrium model when time-scales related with the dune erosion and recovery are considered. The results showed that the dune system affects the beach profile evolution both spatially, with different impacts at different elevations along the cross-shore profile, and temporally, by periodically redistributing the sediment in the system.

**Plain Language Summary** Changes in the shoreline position are the result of a delicate balance between hydrodynamic (e.g., waves, currents, and water levels) and morphology (e.g., dunes, beachface). Dunes are a natural barrier to storms and much of their ability to stand erosive events is related to their recovery after a storm. At the same time, the beachface often responds to incoming waves by either changing its slope (rotation mode) or by advancing/retreating (translation mode). Using 15 years of profile measurements at Vougot beach, France, we identified the different modes and observed if, when and how they occur. Our analysis shows that the evolution of the beach system was controlled by the sediment exchanges and redistribution between the dune and the intertidal beach. Different elevations of the intertidal beach profile showed distinct behavior and different time-scales of change. Our work provides evidence that a multi-temporal scale approach is necessary to predict sediment redistribution along the beach profile.

### 1. Introduction

Over the last few years, research efforts to understand and predict shoreline evolution have increased because of the increased threat posed by climatic changes, including changes in sea levels as well as changes in storm magnitude and frequency. Sediment exchange across the beach occurs over different time-scales, and many uncertainties in the beach/dune response to different drivers still exist on scales ranging from storms to the overall wave climate. The processes involved are further complicated by the stochastic nature of the forcing and the inherent nonlinear interactions and feedbacks operating over multiple temporal and spatial scales (Hapke et al., 2016; Larson & Kraus, 1995).

It is becoming increasingly clear that due to climatic changes coastal erosion is likely to be exacerbated. Sea-level rise (SLR) has been the focus of the attention of the beach community in the last couple of decades (Le Cozannet et al., 2019; Nicholls & Cazenave, 2010), but it is becoming evident that shoreline erosion is

not only affected by SLR but also by changes in the (storm) wave climate (Masselink, Castelle, et al., 2016). For example, Barnard et al. (2015) found that El Niño and La Niña events in the Pacific Ocean basin might lead to extreme coastal erosion and flooding, independent of SLR. The importance of storms was also reported along the Atlantic Coast of Europe during the 2013/2014 winter, which was the most energetic winter since 1948 (Masselink, Scott, et al., 2016; Matthews et al., 2014) causing unprecedented dune and beach erosion on Northern European Atlantic beaches (Blaise et al., 2015; Burvintg et al., 2018; Castelle et al., 2015; Dissanayake et al., 2015; Masselink, Scott, et al., 2016; Pérez-Alberti & Trenhaile, 2015). Therefore, models that can accurately predict shoreline changes over both short (storm) and mid horizons (wave climate) are required. D'Anna et al. (2020) studied the uncertainty associated with different variables using a cross-shore-only version of the LX-Shore shoreline change model (Robinet et al., 2018) where SLR effects are included using the Bruun Rule. When applied to reproduce 20 years of shoreline evolution at Truc Vert beach, France, they found that the free parameters (response rate, linear trend, and beach memory) used to model intra to multi-annual time-scales resulted in larger contributions to the overall uncertainty than the SLR or depth of closure (used in applying the Bruun Rule). This highlighted a major problem in long-term predictions, since climate change may significantly impact the wave climate and the extremes, complicating the use of model parameters calibrated using past data (D'Anna et al., 2020).

During storms, the shoreline typically moves landward (erosion), while during calm periods the shoreline typically moves seaward (accretion). Shoreline changes occurring over much larger time-scales (decadal to centennial) may be the result of other factors such as longshore sediment transport, changes in sediment supply, anthropogenic interventions, SLR, and changes in the wave climate, amongst others (Bruun, 1988; Hanson, 1989; Vitousek et al., 2017). Generally, cross-shore sediment transport is considered to be the main control of shoreline evolution at seasonal and inter-annual time-scales (Kriebel & Dean, 1985; Miller & Dean, 2004), whilst longshore processes (specifically on open coastlines) become dominant over much longer time-scales (decadal to centennial; Ashton et al., 2001; Hanson, 1989; Hurst et al., 2015). Nonetheless, factors such as chronological order of storms (Callaghan et al., 2008; Coco et al., 2014; Senechal et al., 2015), phase of the tide (Castelle et al., 2014; Lemos et al., 2018), and variable water levels (Ruggiero et al., 2001; Serafin & Ruggiero, 2014) may also have an important role in interpreting dune/beach coupled dynamics. In addition, the antecedent morphological conditions, such as, shoreline orientation and exposure to incoming waves, bar morphology among others, may also have significant impacts on the shoreline response (Blossier et al., 2017; Castelle et al., 2010; Davidson et al., 2013; Miller & Dean, 2004; Yates et al., 2009).

Uncertainties in the prediction of dune/beach system changes are still large due to limited knowledge of the interactions between the physical drivers and the system response, which occur over a range of time-scales. For instance, short-term dune/beach erosion during storms may cause abrupt changes to the coastal system with long-lasting effects. Drivers that control dune/beach erosion and subsequent recovery are likely to be different, and therefore the time-scales associated with such processes will also be different. For example, erosion is usually fast and episodic (hours to days), while recovery is often slow and long-term (months to years), and the physical processes and therefore time-scales are different for dunes and beaches (Burvintg et al., 2018; Dodet et al., 2019). Recently, Conlin et al. (2020) used hybrid Surface Empirical Orthogonal Functions to show that storm impacts can generate persistent topographic features that remain visible for months to years, generating a feedback that influences the response to future storms along different portions of the elevation profile as well as the alongshore variability. This can overwhelm the seasonal topographic signal associated with seasonality in water levels and storminess.

Dune erosion has been found to be a result of wave and water level action mobilizing and removing sediment from the dune/berm and depositing it offshore. Nonetheless, Cohn et al. (2018) found that high water levels, along with wind-induced sediment transport, may also contribute to dune growth. Erosion along the upper beach has been attributed mainly to interactions between the impacts of incident waves and the antecedent morphology of the sub-aerial and subaqueous beach (Coco et al., 2014; Splinter et al., 2014). In addition, dune recovery by wind-blown sand occurs over significantly longer time-scales compared to the recovery of the upper beach (Morton et al., 1994; Phillips et al., 2019).

Although the external drivers that control dune and beach erosion and subsequent recovery may vary, feedbacks between both parts of the dune/beach system play an important role. For dunes to recover, a sediment supply source is needed. This requires that the beach recovers, through the onshore migration and welding

of nearshore bars, which is in turn followed by accretion along the backshore to generate a sediment source for dune recovery (Houser, 2009; Larson et al., 2016). On the other hand, dune erosion is controlled not only by the duration of time that wave run-up reaches the dune toe, but also by the width of the beach immediately fronting the dune, since the berm reduces the wave energy reaching the dune (Beuzen et al., 2019; Houser, 2009; Plant & Stockdon, 2012).

In recent decades, data availability has increased, with long time-series from camera systems (Montaño, Blossier, et al., 2020; Phillips et al., 2017), LiDAR measurements (Phillips et al., 2019), advances in satellite remote-sensing (Luijendijk et al., 2018; Vos et al., 2019), or longer time span topo-bathymetric measurements (Ludka et al., 2019; Turner et al., 2016) encouraging the development of shoreline change models using data-driven approaches. For instance, equilibrium models (Davidson et al., 2013; Yates et al., 2009), also called Hybrid models (Montaño, Blossier, et al., 2020), have become popular due to their simplicity, low computational cost, and good performance in predicting shoreline changes at intra-annual to multi-annual time-scales. This type of model is based on the dis-equilibrium concept (Wright et al., 1985), in which the shoreline position rate of change is governed by the difference between present and equilibrium wave and/or morphological conditions (Davidson et al., 2013; Miller & Dean, 2004; Yates et al., 2009). This type of model relies heavily on data to search for and optimize the model free parameters (Splinter et al., 2013). As one might expect, the performance of these cross-shore models is poor at locations where the driver of shoreline changes is long-shore sediment transport (Dodet et al., 2019). To fill this gap, Vitousek et al. (2017) added a new term to the cross-shore model based on Yates et al. (2009). The new term accounts for long-shore processes through a “one-line” model approach (US Army Corps of Engineers, 1984). The authors also added a term that accounts for SLR-induced shoreline recession based on the “Bruun rule” (Bruun, 1962), in addition to a long-term trend term taking into account unresolved processes. Robinet et al. (2018) followed a similar approach and proposed a model integrating the cross-shore component based on the ShoreFor model of Davidson et al. (2013), which also includes a long-term trend term, and an alongshore component similar to Ashton et al. (2001). A more recent improvement to this type of model was introduced by Antolínez et al. (2019), which included the contribution of foredune erosion, in addition to the cross- and long-shore changes. Despite the level of complexity of the model, the berm profile was fixed, and dune recovery was neglected. Other types of more complex process-based models calculating 2D or 3D sediment transport processes have been proposed to simulate dune/beach changes from intra-annual to multi-annual temporal scales (Hanson et al., 2010; Larson et al., 2016; Palalane et al., 2016). However, their applicability remains to be tested, and in some cases, process-based models have not shown better performance than simpler equilibrium-based hybrid models (Splinter & Palmsten, 2012).

Hapke et al. (2016) found that shoreline change patterns representing responses to different oceanographic forcing factors can often be separated, and shoreline response can be resolved on time-scales ranging from storm events to decadal variations. Montaño et al. (2021) presented a different approach to equilibrium models in which shoreline changes are predicted by isolating and associating time-scales in the drivers and the shoreline response. The method hypothesizes that shoreline changes at a specific time-scale can be predicted using the drivers at the same temporal scale. For instance, seasonal shoreline changes might be predicted using only seasonal oscillations in the drivers while the total shoreline change results from the summation of different time-scales (e.g., seasonal, annual, bi-annual, and decadal). As in equilibrium models, this approach heavily relies on data to identify the important time-scales and to calculate the free coefficients that link drivers and shoreline response at different time-scales. This model approach also uses the sea-level pressure (SLP) fields and gradients to predict the shoreline changes, since SLP might contain information not present in the bulk waves parameters ( $H_s, T_p, \theta$ ), such as, mean water level fluctuations, wave generation areas, and information of large atmospheric anomalies.

Models of shoreline evolution often struggle to link observed changes to the incident wave field. We hypothesize that because of the many timescales involved, shoreline evolution models fail to capture the dynamic form of the beach (which reflect stored mass, or enhanced dissipation) and, in particular, the role of dune-beach interactions in the profile response to specific events. The aim of the present study is to analyze dune-beach behavior in the context of shoreline modeling, using almost 15 years of observations of monthly subaerial beach/dune profiles collected in a macro-tidal beach, Vougot, France (Suarez, Blaise, Cariolet, et al., 2016; Section 2.1). To do so, the SPADS (Shoreline Prediction At Different time-Scales)

model (Montaño et al., 2021) is used to analyse the dominant time-scales of observed changes at different elevations along the intertidal profile and predict shoreline changes (Section 2.2). The beach migration modes (steepening, flattening, advance, and retreat) were identified through a profile centroid analysis (Section 2.3). Results of both the analysis and the shoreline predictions using SPADS are presented and discussed in Sections 3 and 4, where the influence of dune events on shoreline changes and the implications for the shoreline modelling are also discussed. Finally, the key findings and conclusions are summarized in Section 5.

## 2. Methods

### 2.1. Study Area

Vougot is a ~2 km long beach located on the north coast of Finistère in Brittany (France) in the municipality of Guisseny (Figure 1a). The beach is characterized by a macro-tidal range, reaching 8.5 m (referring to astronomic tide), which can expose more than 400 m of the intertidal profile at low tide. The beach is backed by an extensive dune system that varies from 200 to 400 m wide, with a dune sediment size  $D_{50} \sim 0.20$  mm, which becomes coarser on the beach ( $D_{50} \sim 0.25 - 0.315$  mm). The beach is fronted by a rocky shore platform with the presence of islets and reefs that shelter the coast, giving the dune system a convex curved shape (Suanez et al., 2012).

Monthly sand level observations of the sub-aerial beach/dune profile (Figure 1f) from nearly 15 years (2004/07/05 to 2018/12/11) were collected using a DGPS Trimble 5800/5700 and a Topcon HYPER-II, in RTK mode with errors reaching up to  $\pm 5$  cm in  $x$ ,  $y$ , and  $\pm 2$  cm in  $z$ . Data were analyzed for three profiles located in the eastern part of the beach, near the jetty of Curnic, which connects the Enez Croaz-Hent islet to the coast (Figure 1b, red lines). Although the shoreline is generally defined as the physical interface between land and water (Boak & Turner, 2005), on macro-tidal beaches where the cross-shore length is of the order of hundreds of meters, an exact shoreline definition is difficult to obtain (Castelle et al., 2014). In this study, different elevations are used as a proxy for the shoreline cross-shore position ( $S = f(z)$ ) where  $z$  represents the different elevations. Temporal changes in contour elevations “shoreline”, each 0.5 m are displayed in Figure 1f, left panels.

In recent decades, the dune system experienced significant retreat, especially along the eastern part of Vougot beach, with most of the material transported to the west, contributing to building up the western section of the beach (Suanez et al., 2010, 2012). This erosion has been attributed to the construction of the jetty of Curnic in 1974, which modified the local hydrodynamics, interrupting the westward sand drift and inducing a scarcity of sediment over the eastern, downdrift part of the Vougot beach/dune system. In addition, the beach is characterized by a rocky platform in the tidal zone, with relief in form of small islets and reefs that cause wave diffraction and complex current patterns, especially impacting longshore currents (Suanez et al., 2010, 2012). Along the three analyzed profiles, the presence of different types of “hard bottom” (red lines, Figure 1f, right panels), for example, periglacial deposits (clay), rocky or peat outcrops, or Pleistocene/Holocene gravel accumulation, limits sand availability. During some periods of the year, these hard surfaces are no longer covered by sand, especially along the lower part of the profiles.

Suanez et al. (2012) carried out a detailed analysis of the dune recovery after the storm “Johanna” hit the French Atlantic coast on March 10, 2008, which caused severe dune erosion (Figure 1c; Suanez & Cariolet, 2010). The subsequent phase of dune recovery, which lasted from 2008 to 2013 (Figure 1d) was characterized by the growth of vegetation and the construction of “secondary” embryo dunes, which reduced the impact of the storm surge. Another severe dune erosion event occurred during the 2013/2014 winter (Figure 1e), considered one of the most energetic winters along the Atlantic coast of Europe since 1948 (Masselink, Scott, et al., 2016). Three energetic winter storms (January, February, and March) coincided with large spring high tides, augmenting the effects of the storm surge, with important implications for the dune-beach system (Blaise et al., 2015; Masselink, Scott, et al., 2016; Suanez, Blaise, Cancouët, et al., 2016). The current study evaluates both dune erosion events and the subsequent recovery phases.

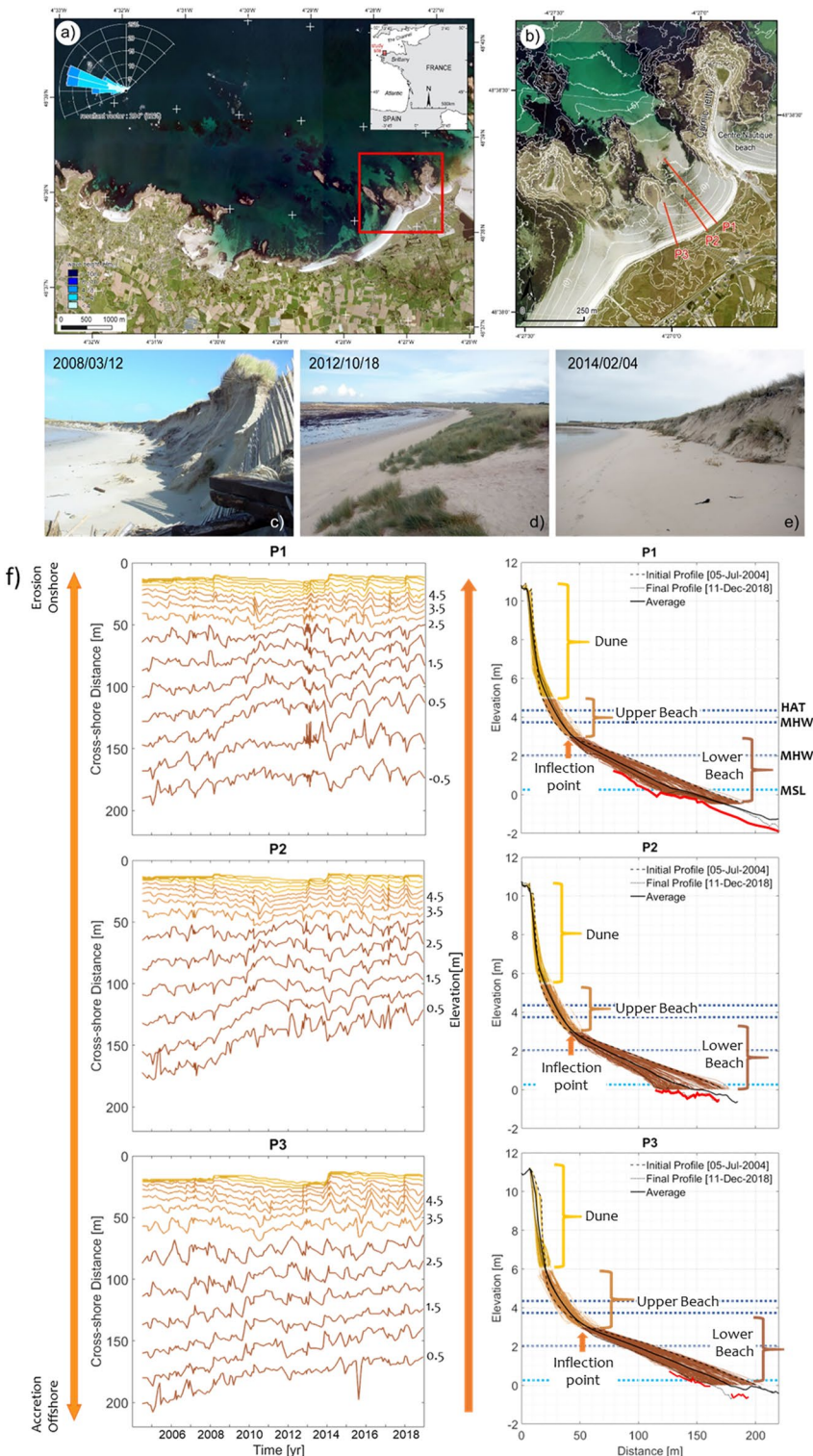


**Figure 1.** Study site. (a) Location of Vougot beach, France, with the location of the modeled waves (wave rose; blue dot); (b) Detail of Vougot beach identifying the three profiles (red lines) analyzed in this study; (c) Dune erosion event: March 12, 2008; (d) Dune recovery: October 18, 2012; (e) Dune erosion event: February 04, 2014. (f) Contour elevation position time series (left panels) for elevations ranging from lower intertidal zone to over upper intertidal zone and dune. Beach profile evolution during the study period (2004–2018) along the intertidal zone (right panels) for Profile 1 (P1), Profile 2 (P2), and Profile 3 (P3). Red lines represent the hard bottom (clay and/or rocky and/or peat outcrops). Dashed dark blue lines represent the Highest Astronomic Tide (HAT), Mean High Spring (MHWS), and Mean High Water Neap (MHWN), respectively. Dashed light blue lines represent the Mean Sea Level (MSL). Images a and b Institut National de l'Information Géographique.

## 2.2. The SPADS Model

Montaño et al. (2021) introduced and tested a new model for Shoreline Prediction At Different time-Scales (SPADS) based on identifying the time-scales of drivers and shoreline change using the Complete Ensemble Empirical Mode Decomposition (CEEMD) method (Huang et al., 1998; Torres et al., 2011), and then linking the resulting time-scales with calibrated parameters. The model showed good performance compared with a traditional equilibrium model when tested at two cross-shore dominated beaches (Narrabeen, Australia and Tairua, New Zealand). CEEMD is a noise-assisted data analysis approach based on the empirical mode decomposition (EMD) introduced by Huang et al. (1998). EMD-based methods were designed to identify nonlinear and non-stationary oscillations in data, assuming that simple oscillatory modes of significantly different superimposed frequencies coexist (Huang et al., 1998). EMD decomposes time series into a finite set of “intrinsic mode functions” (IMFs), representing different time-scales with varying amplitudes and frequencies (the last IMF is considered to be the trend). CEEMD improves on EMD, by assisting the IMF separation through the addition of Gaussian white noise to the signal and the true IMF is calculated as the mean of an ensemble (100 realizations in our study).

Modeling with SPADS consists of a number of steps, starting with the decomposition of the time-series of shorelines and drivers using the CEEMD method. Then, a statistical test (Wu & Huang, 2004) is applied to identify the significant IMFs obtained using the CEEMD approach (only the IMFs that satisfied a significance level higher than 95% were selected for further analysis). The reconstruction of the shoreline changes at each individual time-scale is performed through an optimization analysis to find the coefficients that link driver and shoreline changes by maximizing the Mielke's modification index  $\lambda$  (Duveiller et al., 2016). The total shoreline position is reconstructed as the summation of the different time-scales. The CEEMD method needs to be run multiple times with different white noise initializations (we used white noise amplitudes between 0.1 and 0.5 of the signal standard deviation). The final shoreline position is the average of the shoreline positions obtained with the different levels of white noise. The SPADS model uses two type of drivers: large-scale two-dimensional SLP fields and gradients from Climate Forecast System Reanalysis (CFSR), and wave bulk parameters. The first step to obtain the SLP information is to find the influence area with the ESTELA (Evaluating the Source and Travel time of the wave Energy reaching a Local Area) method (Pérez et al., 2014). This method evaluates the source and travel time of waves reaching a given location based on the geographic criteria and the two-dimensional wave spectra (see Rascle & Arduuin, 2013). In order to account for the travel time of swell waves in the analysis, the SLP information is modified according to the isochrones of the average travel time as in Hegermiller et al. (2017) (Figure 2a). After the SLP field and gradients is modified with the ESTELA method, a principal component analysis (PCA), a statistical technique widely used in climatology to identify dominant variability patterns and reduce dimensionality (Camus, Menendez, Izaguirre, et al., 2014; Rueda et al., 2019) is performed.

The PCA projects the original data on a new space, searching for the maximum variance of the sample data. The dominant spatial variability patterns, called empirical orthogonal functions or EOFs (Figures 2b and 2c), and temporal coefficients, that is, principal components or PCs (Figures 2d and 2e), are used to reconstruct the original predictor  $X(x, t)$  with a linear combination of EOFs and PCs, where  $N$  is the number of selected EOFs:

$$X(x, t_i) = EOF_1(x)PC_1(t_i) + EOF_2(x)PC_2(t_i) + \dots + EOF_N(x)PC_N(t_i) \quad (1)$$

Following Montaño et al. (2021), we only used the first 10 PCs (i.e.,  $N = 10$ ), which explain up to 54% of the overall variance. As discussed in Montaño et al. (2021), this analysis including the use of SLP and its gradients allows tracking wave information from a large generation area, avoiding reducing the large-scale variability to a single bulk wave parameter, which would ignore the complexities of the wave spectra. For example, it would ignore wave bi-modality which has been found important in different coastal processes, such as run-up and beach rotation (Montaño, Blossier, et al., 2020; Wiggins et al., 2020). On the other hand, the wave information considers bathymetric effects that are not captured by SLP. Thus, in this study both drivers are used to predict shoreline changes. As discussed in Montaño et al. (2021), the model allows inclusion of any driver relevant for shoreline prediction (e.g., waves, winds, and water levels) at both local and regional scales. More information about the model development can be found in Montaño et al. (2021).

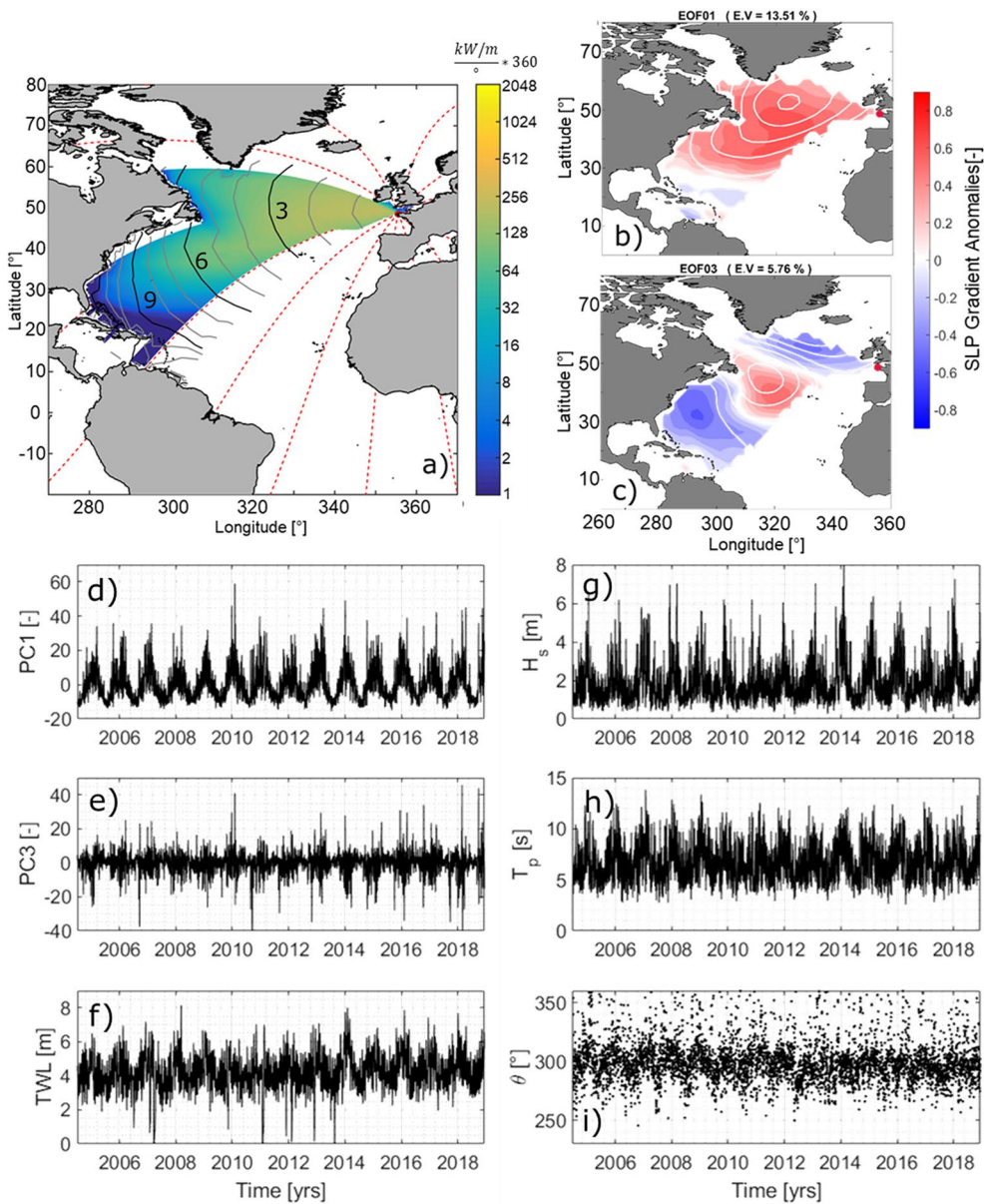


**Figure 2.** Model Drivers. (a) mean energy flux for all possible source points (calculated using ESTELA). The travel time (in days) is represented by the black lines (3-day increments) and gray lines (1-day increments). Red dotted lines represent the great circles; (b) and (c) are examples of the first and third empirical orthogonal functions (EOFs) of the SLP fields and gradients. Shaded areas represent SLP gradients, while the contours represent SLP fields; (d) and (e) are examples of the corresponding principal components (PCs) for (b) and (c) used as drivers for the CEEMD model; (f) total water levels (TWLs) and (g)–(i) bulk wave bulk parameters used for the analysis ( $H_s, T_p, \theta$ ).

Wave parameters in 43 m water depth (Figure 1a) were obtained using the numerical model WaveWatch3 run by the Ifremer (Boudière et al., 2013) (Figures 2g–2i). As can be seen in Figure 1a, waves arrive principally from the northwest (2004–2019). The beach is partially sheltered from the direct impact of Atlantic swell, and relatively well protected from waves originating in the west to northwest by an offshore platform scattered with islets and reefs that emerge at low tide (Masselink, Scott, et al., 2016; Suanez et al., 2012). Since dune erosion events are important at Vougot, the total water level (TWL) is also included in the analysis, with tide measurements from the Roscoff tide gauge station located about 30 km to the east of the survey area (Suanez et al., 2012). The maximum wave run-up ( $R_{max}$ ) was computed using an existing formula provided by Cariolet and Suanez (2013) and Suanez et al. (2015), which has been calibrated

using field measurements for Vougot Beach as,  $R_{max} = 0.68H_0\xi_0$ , with  $\xi_0 = \tan\beta/\sqrt{H_0/L_0}$ , where  $H_0$  and  $L_0$  are the offshore wave height and wave length, and the beach slope  $\beta$  corresponds to the active section of the upper part of the beach, which in macro-tidal environments was found to estimate more accurately run-up predictions (Cariolet & Suanez, 2013).

To analyze the influence of the different time-scales on shoreline prediction, we compared the SPADS model with the ShoreFor model (Davidson et al., 2013). ShoreFor is one of the most widely applied shoreline models due to its simplicity and high performance (Dodet et al., 2019; Montaño, Coco, et al., 2020; Splinter et al., 2014). The model is based on the equilibrium concept so that cross-shore changes in the shoreline position are proportional to the incident wave power and the degree of disequilibrium. For wave conditions more energetic than equilibrium the beach is eroded and vice-versa. The model has two free parameters: a disequilibrium term that depends on the “memory decay” of the beach (related with the dominant time-scale) and a linear trend term that accounts for additional processes not directly included in the model formulation (e.g., longshore sediment transport). Detailed information about the ShoreFor model can be found in Davidson et al. (2013)

### 2.3. Centroid Analysis of Beach Profile Changes

In general, four principal modes of adjustment can be identified for any beach profile: flattening and steepening (cross-shore beach profile rotation around a pivot point, Figure 3a quadrants I and III), and advancing and retreating (cross-shore beach profile translation, Figure 3a, quadrants II and IV). These principal modes can also be combined to give more complex modes of rotation and translation, as observed on many coasts (Soulsby et al., 1999; Townend et al., 1990).

In the rotation modes, the cross-shore profile does not retreat or advance as an equilibrium profile but evolves toward a flatter or steeper profile around a pivot point (nodal point). The flattening mode consists in upper beach erosion and lower beach accretion causing a decrease in the beach slope, while the steepening mode displays the opposite behavior (upper beach accretion and lower beach erosion, causing an increase in the beach slope). In the translation modes, the beach profile response is vertically uniform, and no pivot point is observed (see the schematic in Figure 3a). In addition, steepening/flattening can occur with no net change in profile volume, whereas retreat/advance implies a change in volume within the control volume. Although migration modes generally have been computed using beach volumes (e.g., Burvingt et al., 2017), a volumetric centroid analysis was used here to estimate beach migration modes following Taylor et al. (2004) and Villamarín (2017).

The centroids, here defined as a measure of the volumetric center of the profile, were computed using the CoastalTools package (Townend, 2018). Cross-shore variations of the centroid (X horizontal axis) and vertical centroid variations (Z vertical axis) are computed from the first moments calculated using the cross sectional control area defined by a rectangle (Figure 3b). Inside the control area, the following parameters are calculated:

$$\text{Volume: } V = \int z' dx \quad (2)$$

$$\text{Horizontal centroid: } X = \int x' z' dx / V \quad (3)$$

$$\text{Vertical centroid } Z = \int x' z' dz / V \quad (4)$$

where  $x'$  and  $z'$  are the horizontal and vertical distance from the origin ( $x_{min}, z_{min}$ ) of the control area (Figure 3b):

$$x' = x - x_{min}; x' \geq 0 \text{ and } z' = z - z_{min}; z' \geq 0 \quad (5)$$

The total beach and dune volumes were computed using the defined control area ( $V_T$ , black dashed square and  $V_D$ , red dashed square, Figure 3b). These areas were based on the lower limits of the survey data, with  $x_{T, min} = 0 m$  for the three profiles, and with  $z_{T, min} = 0.5 m$  for Profile 1 and  $z_{T, min} = 0 m$  for Profiles 2 and 3. The intertidal volumes considered here are likely to be less than the total sediment volume out to the closure depth and may not represent the total nearshore sediment volume. For the dune control area, we assumed that the dune toe elevation remained fixed based on the field observation for the initial measurement (red dot, Figure 3b). Then,  $x_{D, min} = 0 m$  for the computation of the dune volumes at the three profiles, while

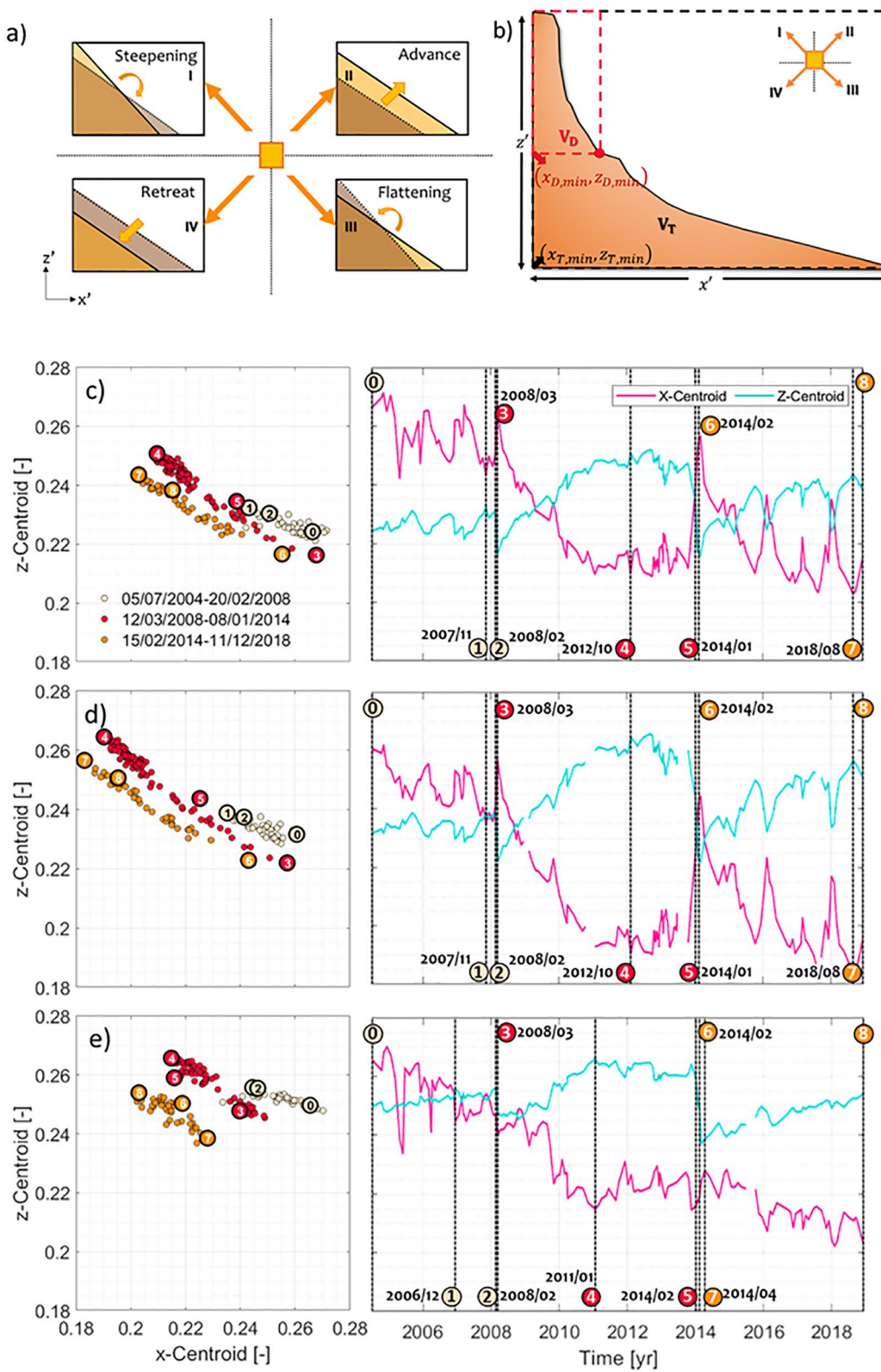


Figure 3.

$z_{D, \min} = 5 \text{ m}$ , ( $x = 18 \text{ m}$ ) for Profiles 1 and 2, and  $z_{D, \min} = 5.6 \text{ m}$ , ( $x = 21 \text{ m}$ ) for Profile 3 based on the dune toe location in the initial measurements.

With the aim of comparing directly different profiles, the non-dimensional centroid coordinates  $x_l$ ,  $z_l$  are computed as:

$$\text{Non-dimensional volume: } m_0 = \int z'' dx'' \quad (6)$$

$$\text{Non-dimensional horizontal centroid: } x_l = \int x'' z'' dx'' / m_0 \quad (7)$$

$$\text{Non-dimensional vertical centroid } z_l = \int x'' z'' dz'' / m_0 \quad (8)$$

where  $x''$  and  $z''$  are defined as:

$$x'' = \frac{x'}{L_x} \text{ and } z'' = \frac{z'}{L_z} \quad (9)$$

with  $L_x = \max(x')$  and  $L_z = \max(z')$

### 3. Results

#### 3.1. Dune Influence on Shoreline Behavior

Through the non-dimensional centroid maps, three “clusters” were identified for the three profiles when the entire beach control area ( $V_T$ ) is used (color dots, Figures 3c–3e). We use the word cluster to indicate periods in time when the beach adjustment is associated with a particular trend (steepening interval), distinct from the translation (net erosion) that occurs between clusters. Each cluster has numbered events of notable change that represent the date when the cluster initially appeared, the most extreme migration event, and the date of the last observation before the system shifted to a different cluster (Figures 3c–3e). By analyzing the overall alignment of the clusters and the steps between each cluster (Figures 3c–3e, left panels), the behavior of the beach can be interpreted based on the modes defined in panel (a). Only profile changes (Figures 4 and 5) for Profiles 1 and 3 are shown, since the centroid analysis displayed different chronologies (Figures 3c–3e, right panels) and beach behavior for the Profiles 1 and 2 are characterized by very similar dynamics. Figures 3c and 3d (left panels) show that all three profiles never return to an earlier cluster (steepening interval), but rather shift diagonally toward quadrant IV (i.e., retreat), indicating that whole profile is losing sediment. This separation between clusters in the direction of the quadrant IV was more evident for Profile 3, which experienced the largest loss of sediments (Figure 6).

The primarily diagonal movement toward the quadrant I within each cluster indicates the dominance of steepening, while the changes from the last date of one cluster to the first date of the following one, mainly correspond to steps toward the quadrant III (Profiles 1 and 2), indicating significant flattening events (Figures 4d and 4g). Nonetheless, during the first large dune erosion event attributed to the March 10, 2008 “Jo-hanna” storm, Profile 3 showed a movement toward the quadrant IV, indicating beach retreat (Figure 5d).

The first cluster in all three profiles (beige dots) corresponds to the period from the beginning of the measurements (2004/07, see label 0) to the last date before a shift to a different cluster (2008/02, see label 2). During this period, the three profiles mainly experience profile steepening (e.g., migration toward quadrant I, from label 0 to 1), reaching the maximum steepness (left panels, Figures 3c–3e) for Profiles 1 and 2 in 2007/11 (Figure 4b) and in 2006/11 for Profile 3 (Figure 5b). Other beach movements within the clusters, due to seasonal-annual variations are observed (see dot with label two in Figures 3c–3e, 4c, and 5c), although with less pronounced effects on the beach behavior. On March 10, 2008, the high energy storm Jo-hanna hit the French Atlantic coast causing significant dune face erosion (Suanez & Cariolet, 2010; Suanez et al., 2012), inducing beach changes associated with a new cluster (red dots, Figures 3c–3e, left panels).

**Figure 3.** Beach migration analysis. (a) Diagram of the four primary modes of beach change inferred from the centroid movement. The dotted black line represents the initial beach state (yellow square), while the solid black line represents the subsequent beach state. The four quadrants are used in the interpretation to indicate the  $x$ -centroid and  $z$ -centroid movement between each survey; (b) Control areas for the beach volume and centroid computations: Total volume  $V_T$  (black dashed square) and dune volume  $V_D$  (red dashed square), where the red dot represents the initial dune toe, modified from Townend (2018); (c)–(e) Centroid analysis for profiles 1, 2, and 3, respectively. Left: Non-dimensional centroid maps in the  $x'$ - $z'$  vertical plane. The colors represent the three different clusters identified through the centroid analysis. Right: Centroid evolution in time (corresponding dates in right panels).

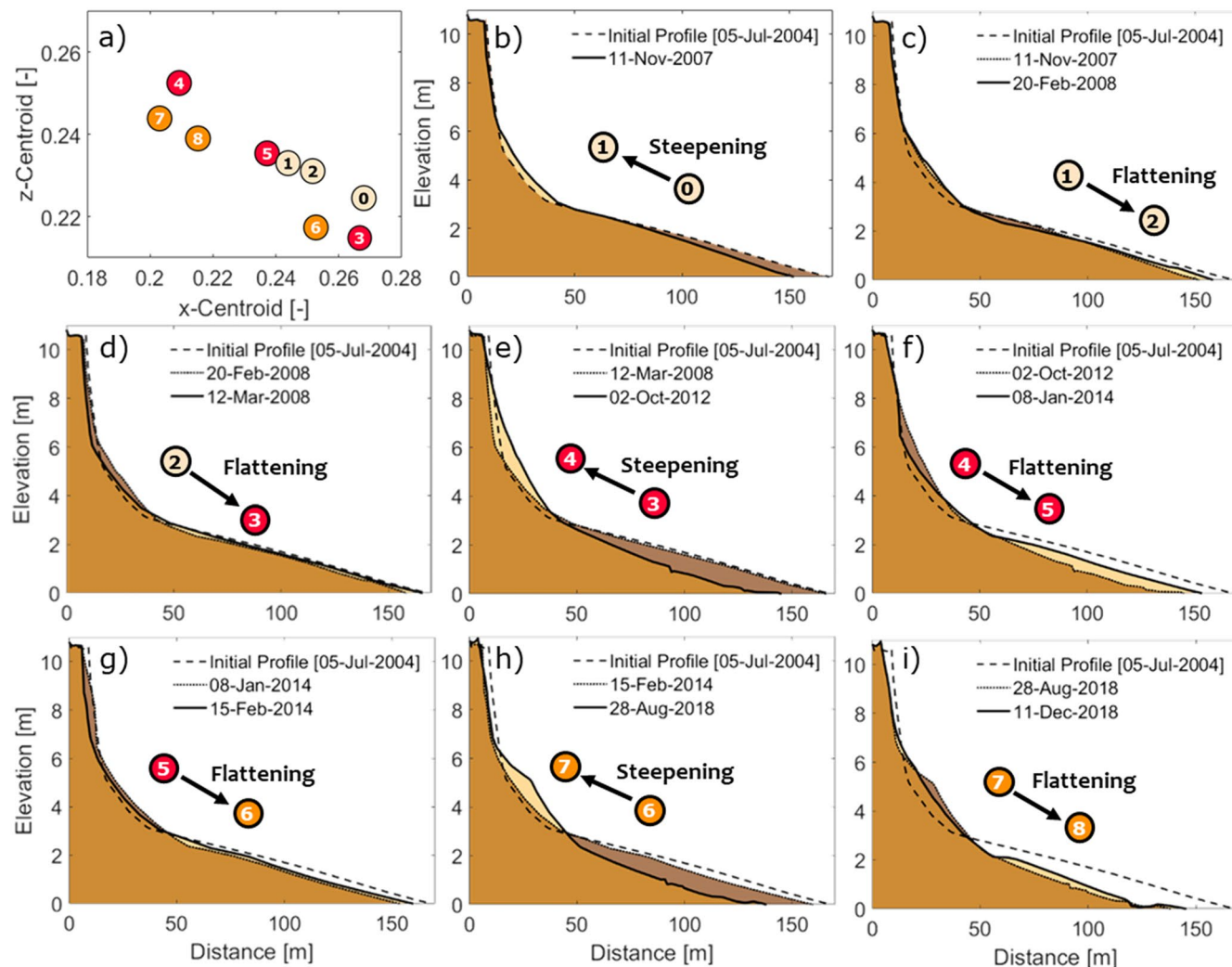


**Figure 4.** Beach changes in Profile 1 corresponding to the non-dimensional centroid analysis in Figure 3c. (a) Non-dimensional centroid map showing the most significant changes only; (b–i) Dune and beach face profiles for each event.

A pronounced flattening (quadrant III migration, labels 2–3, Figures 3c and 3d, left panels) was observed for Profiles 1 and 2 (Figure 4d), and a retreat (quadrant IV) for Profile 3 (Figures 3e and 5d). However, after the storm, the three profiles returned to showing primarily profile steepening (in the quadrant I direction, labels 3–4). The maximum steepening for Profiles 1 and 2 was observed on 2012/10 (label 4, Figures 3c, 3d, and 4e) and on 2011/01 for Profile 3 (label 4, Figures 3e and 5e). As in the first cluster, different migration modes such as flattening, are observed before a change to a new cluster (labels 4–5, Figures 3c–3f, 4f, and 5f). Most of the flattening was caused by a sequence of storms during the 2013/2014 winter that eroded the lower part of the dune, without causing a change in the cluster. From the sequence of storms experienced that winter, only the storm on February 1–2, 2014, during which the dune face was strongly eroded, generated a change to a new the cluster (yellow dots in left panels, Figures 3c–3e). Behavior within this cluster was different for Profile 3, which experienced flattening (labels 6–7, Figures 3d and 5h) and dune face erosion, contrary to profiles 1 and 2. It is plausible that profiles 1 and 2 were already highly eroded due to the February storm, which did not cause a significant erosion in Profile 3.

The right panels in Figures 3c–3e show the x (red lines) and z (yellow lines) centroid evolution over time. The two large erosion events and subsequent recovery of the dune due to the erosion of the intertidal beach changed the beach dynamic. As observed in the left panels, profiles 1 and 2 show similar behavior. Whilst we highlight distinct phases of beach migration mode for the entire beach ( $V_T$ ), Figures 3c and 3d, right

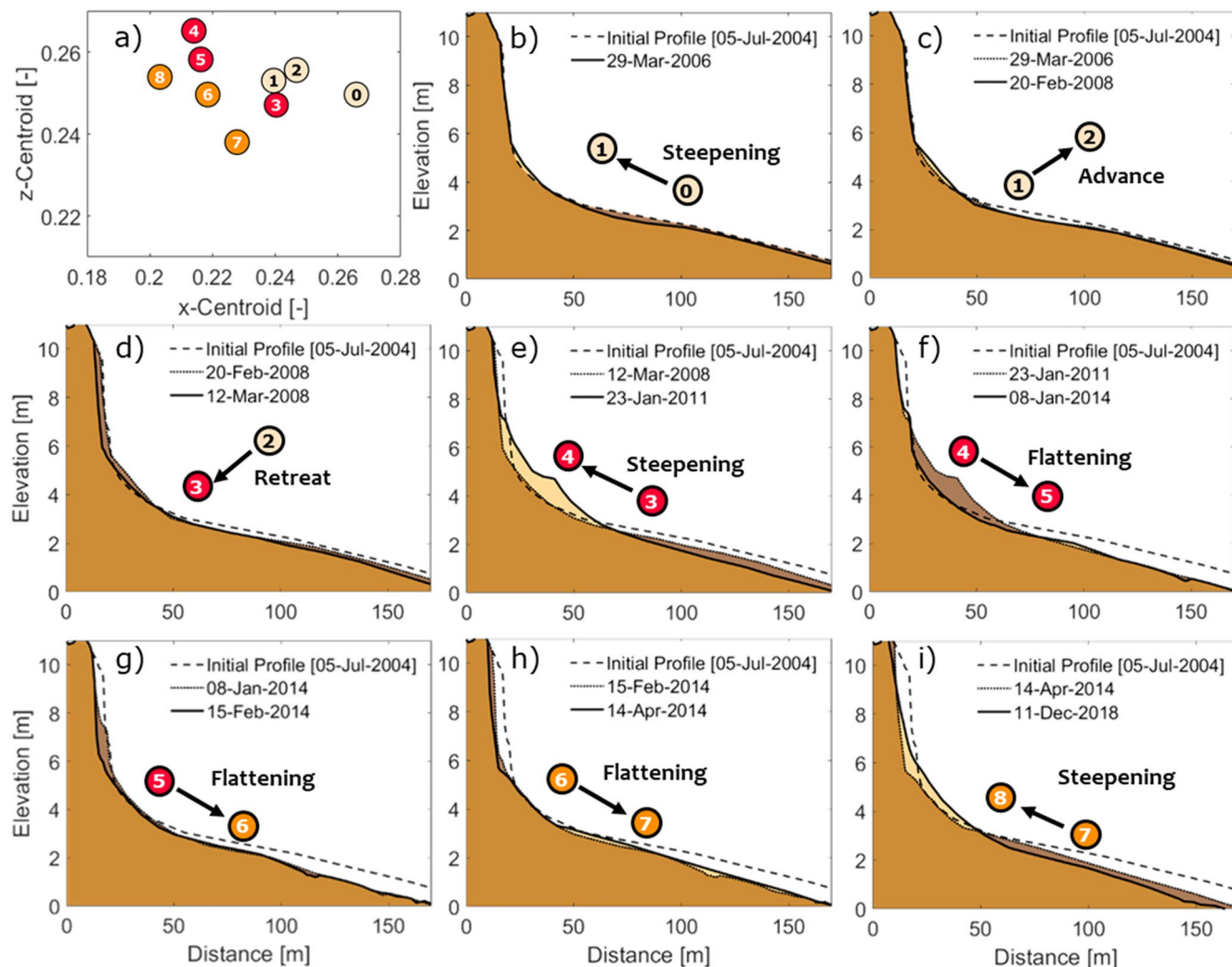
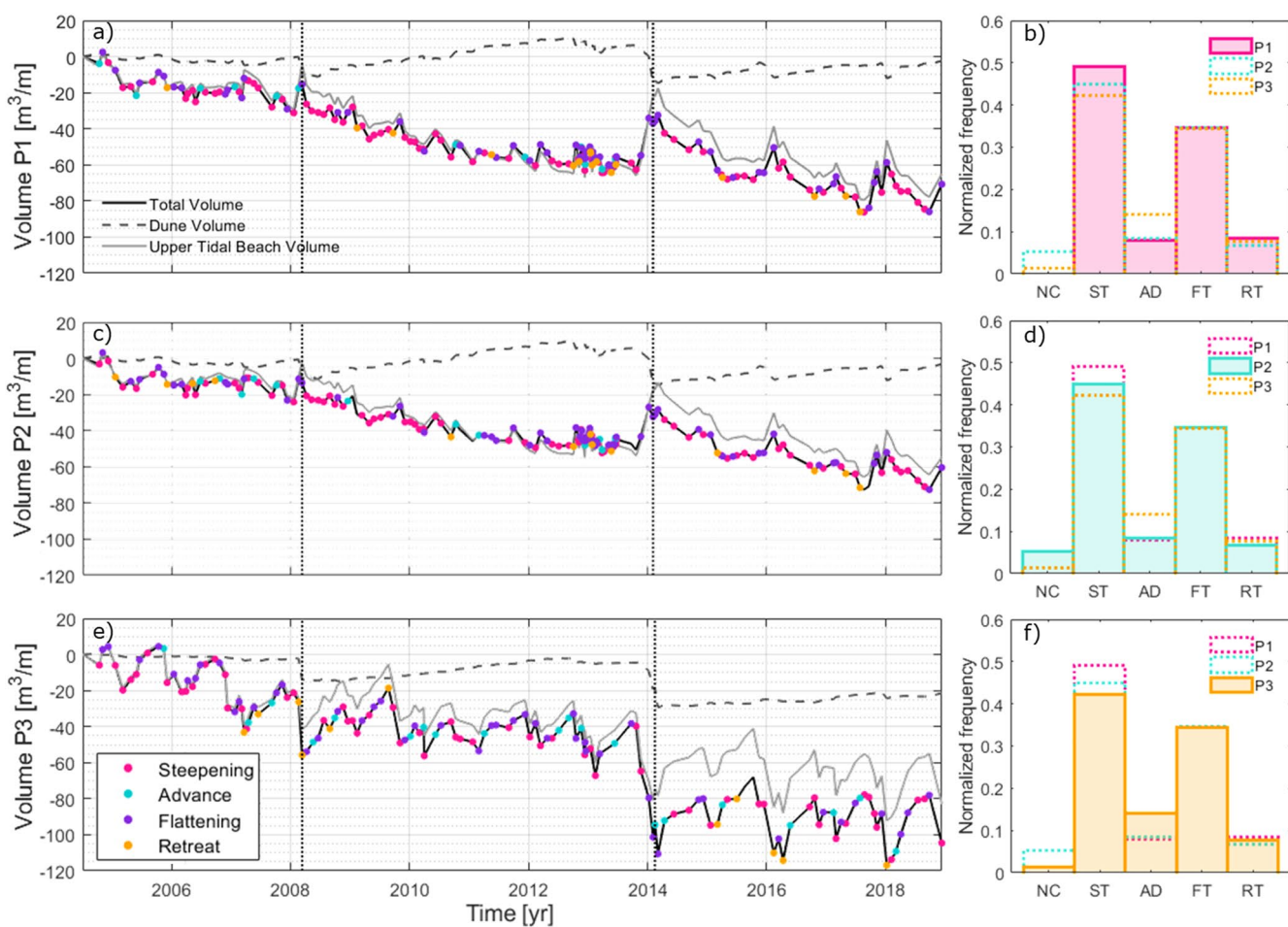


Figure 5. Same caption as Figure 4 but for Profile 3.

panels, show that the  $x$  and  $z$ -centroid, plotted to the same non-dimensional scale, are not always mirrored traces of each other. When they are this implies the dominance of steepening or flattening. However, when the change of both centroids is positive or negative, this implies advance or retreat, respectively. Results show periods of predominant translation modes (retreat/advance) or rotation modes (steepening/flattening), although there are also times when a translation and a rotation mode occur simultaneously.

The total beach volume (dune and intertidal zone, black line, Figure 6, panels a, c and e) during the measurement period showed a decreasing long-term trend for the three profiles, in agreement with the migration between clusters toward the quadrant IV (Figure 3c–3e). Along profiles 1 and 2, the dune had stages of complete recovery when compared with the initial profile (as seen by comparing the dashed line and dotted line in Figure 4f, and as seen by the dashed gray lines in Figure 6). However, the dune in Profile 3 showed a significant loss in volume when compared with the initial profile. Changes in the dune, upper tidal beach, and total volumes also show different behavior for Profile 3. For instance, the two large dune erosion events (labels 3 and 6) resulted in a slight increase in the total sediment volume for profiles 1 and 2, while Profile 3 showed a large volume decrease. This might be explained by the importance of cross-shore sediment exchanges between the inter-tidal beach and dune (and vice versa) for profiles 1 and 2. A stronger annual cycle is observed in Profile 3, although the long-term retreat trend dominated the overall profile change (see Figure 6e). The long-term trend is likely to be due to the longshore sediment transport toward the west (Suanez et al., 2012) due to wave refraction caused by small islands and reefs (see Figure 2b in Suanez et al., 2012).



**Figure 6.** Beach/Dune volumes and different migrations modes in time. (a), (c), and (e) Volume changes for the three profiles: total volume (black line), dune volume (dashed gray line), and upper intertidal beach volume (solid gray line). The colored dots show the occurrence of different migration modes (identified in the legend) over time. (b), (d), and (f) Histograms of the different migration modes for each profile: no change (NC), steepening (ST), advance (AD), flattening (FT), and retreat (RT).

Also, changes in volume along Profile 3 display a clear erosional trend with a superimposed strong annual cycle. Profiles 1 and 2, only showed an annual cycle after the February 1–2, 2014 storm event. The different beach migration modes are identified in each time series, showing variable responses as a function of time (colors, Figure 6a, 6c, and 6e, with legend in e). The histograms in Figures 6b, 6d, and 6f show that the rotation modes, steepening (ST) and flattening (FT), are predominant. However, as explained previously, steepening and flattening modes can occur simultaneously with translation modes (advance and retreat), as observed at Vougot Beach. The dune volume changes show a large dune recovery (2008–2014) for profiles 1 and 2, while the volume increase in Profile 3 was smaller (dashed gray line, Figures 6a, 6c, and 6e).

The dune control area and volume (red square, Figure 3b) are small when compared with the total beach and intertidal volumes. Therefore, the centroid analysis was carried out for the dune and intertidal beach separately to better understand their respective dynamics. In this case, the analysis was performed preserving the dimensions (Equations 2–4), with the aim to observe the magnitude of the centroid displacement (see axes Figure 7). The dune displays opposing behavior to the total beach control area shows flattening (Figure 7, middle and left panels). The clusters in Profile 3 shift to the quadrant IV, much the same as the total beach, implying net retreat. In contrast, profiles 1 and 2 exhibit a form of recovery over the 3 flattening/steepening episodes. This is in broad agreement with the volume analysis for the dune observed in Figures 4a and 4c (sediment recovery) and Figure 4e (loss of sediment).

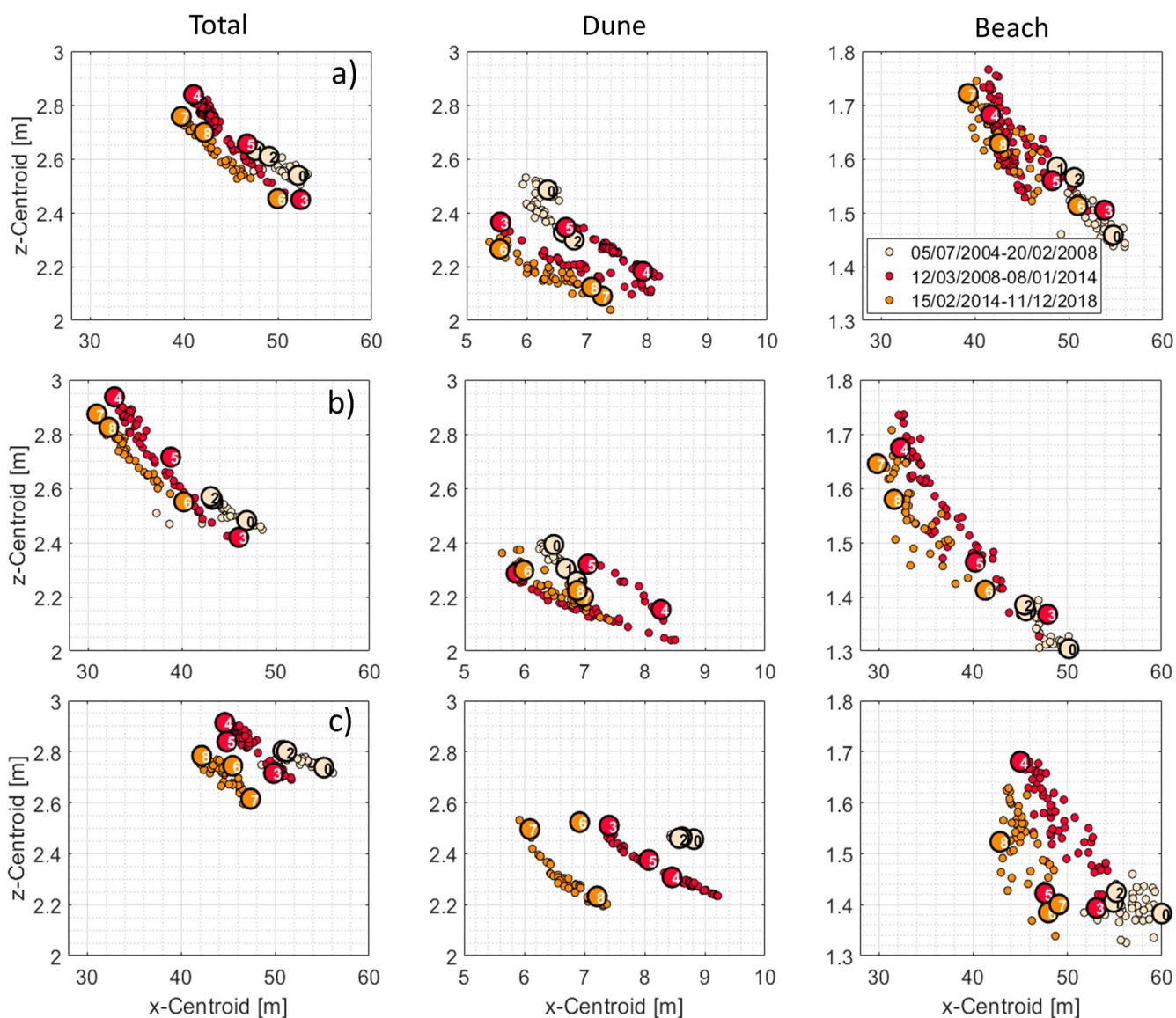


**Figure 7.** Dimensional centroid maps in the  $x'$ - $z'$  vertical plane for (a) Profile one; (b) Profile 2; (c) Profile 3. The colors represent the three different clusters identified through the centroid analysis: (left panels) for the total control area ( $V_T$ ), same as Figures 3c–3e; (middle panels) for the dune control area ( $V_D$ ); and (right panels) for the intertidal beach control area.

When only the intertidal beach is analysed, the cluster separation is less evident for profiles 1 and 2, displaying mainly steepening (in the direction of the quadrant I). This may be explained by the upper part of the intertidal beach gaining sediment from the dune after the two big storm events, as shown in the volume analysis (Figures 6a and 6c, solid gray line), while the lower part of the beach loses sediment. In contrast, Profile 3 showed clearer cluster separation implying intertidal beach retreat (quadrant IV trend), in agreement with the loss of sediment in this zone after the two large storms (Figure 6e, solid gray line). These findings are consistent with Suanez et al. (2012).

### 3.2. Shoreline Evolution and Time-Scales

The centroid analysis shows a dominant steepening trend of the beach during the studied period, with contour elevations retreating strongly along the lower part of the beach and advancing along the upper part of the beach (as seen in Figure 1, left panels and Figures 8c and 8f, lower panels). The analysis also showed

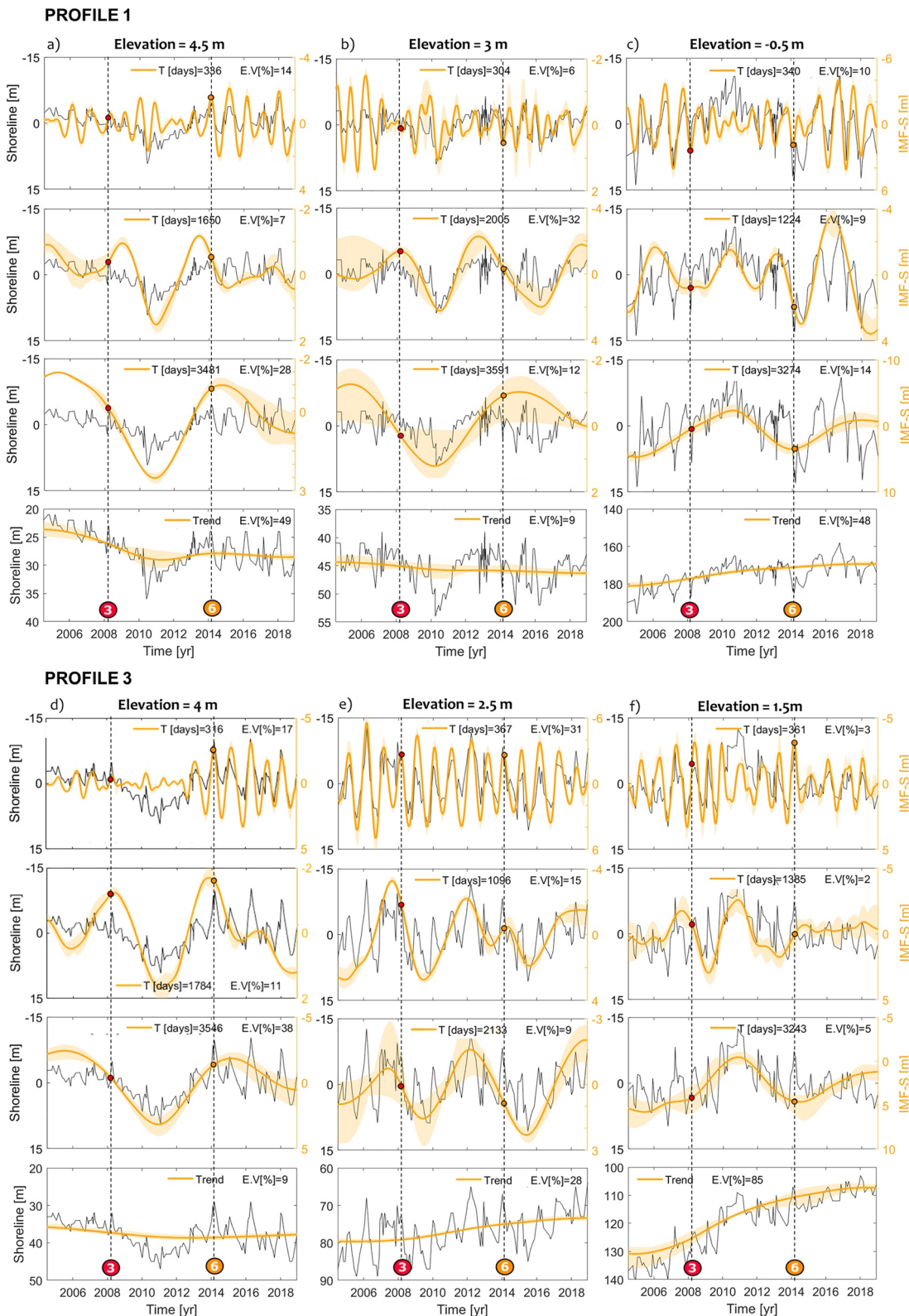


Figure 8.

that the steepening process was interrupted by a strong flattening process during two large dune erosion events in 2008 and 2014, resetting the changes in the shoreline position with a sudden shoreline advance in the lower part of the beach and retreat in the upper part of the beach, especially for profiles 1 and 2. With the aim of analyzing and predicting shoreline changes at Vougot Beach, a recently developed modeling approach SPADS (Montaño et al., 2021) was applied. This approach was tested previously at two cross-shore dominated beaches where dune face dynamics contributed minimally to shoreline evolution, which is in contrast to this site.

For this analysis, the intertidal beaches of profiles 1 and 3 were divided into three sections: lower, middle (a zone around the nodal/inflection point), and upper, since the three selected areas show distinctive behavior (Figure 1f). Figure 8 shows the shoreline trends and the three primary time-scales (IMFs) identified with the CEEMD method (yellow lines, right axis) for both profiles, where the colored dots (labels 3 and 6) indicate the two large dune erosion events. The upper part of the beach in Profile 1 (4.5 m, Figure 8a) is dominated by a long-term accretion trend, which explains up to 49% of the shoreline variance. However, the lower part of the beach showed a strong erosion trend with an explained variance (E.V.) of about 48% ( $-0.5$  m, column Figure 8c). Near the “inflection point” (3 m, column Figure 8b), the long-term trend only explained about 9% of the shoreline variance. The behavior of the trend at the three elevations is in agreement with the dominant steepening mode revealed by the centroid analysis (with significant trends in the upper and lower beach and nearly no trend near the inflection point). In the middle part of the beach, a 2,005-day oscillation, which is on the order of the period between the two large dune erosion events (2,168 days), had the highest E.V. (32%). At all three elevations, an oscillation of about 3,400 days had an important E.V. (12%–28%), in which peaks and valleys are in phase with the maxima of shoreline advances/retreat. In the upper and lower parts of the beach, oscillations with similar time-scales as the duration of the clusters (1,224 days, cluster 1; 1,665 days, cluster 2; and 1,760 days, cluster 3) were also found. In the three sections of the beach, the annual time-scale explained only 13%, 6%, and 10% of the E.V., while the seasonal scale seemed to be important only in the middle part of the beach (14% E.V. not shown). An approximately bi-annual time scale was identified with E.V. lower than 10% for all three elevations (not shown).

Conversely to Profile 1, for Profile 3 the upper part of the beach (4 m, Figure 8d) did not show a strong advancing long-term trend (only 9%), while the middle (2.5 m, Figure 8e) and lower parts (1.5 m, Figure 8f) of the beach experience stronger long-term retreating trends compared to Profile 1 (28%, 85% of the E.V.). This may be explained by the shape of the clusters in Profile 3 (Figure 3e), where the steepening mode (toward the quadrant I) was smaller compared with profiles 1 and 2, while the retreat mode to a new cluster (toward the quadrant IV) was larger. As in Profile 1, temporal scales with a 3,400-day oscillation corresponding to maximum retreat/advance of the shoreline were observed only in the upper and lower parts of the beach. For all three sections of the beach, the oscillations with time-scales similar to the length of the clusters had E.V. of 2%–15%. In the upper part of beach, the annual oscillation showed a significant increase in amplitude after 2014, which was also observed for Profile 1. Also similar to Profile 1, the E.V. in the middle part of the beach (Figure 8e) was distributed more evenly among the different time-scales, with a strong E.V. at the annual scale (31%).

### 3.3. Shoreline Modeling

The shoreline change model was applied at the elevations presented in Figure 8 for profiles 1 and 3.

**Figure 8.** Examples of three dominant shoreline time-scales (top three rows) and the long-term trend (bottom row) identified with the CEEMD analysis for three different elevations. Profile 1 (top) columns: (a) upper (4.5 m); (b) middle, near the inflection point (3 m); and (c) lower ( $-0.5$  m) part of the beach; and Profile 3 (bottom) columns: (d) upper (4 m); (e) middle (2.5 m); and (f) lower (1.5 m) part of the beach. The black line represents the detrended shoreline data (left axis), where small values of the shoreline position represent an eroded state and large values an accreted state. The yellow lines display time oscillations of the IMFs (IMF-S, right axis) after noise averaging, showing the approximate period in days of the shoreline oscillation (T) and the percentage of explained variance (% E.V.). The standard deviation due to different white noise levels is represented by the shaded yellow zone. Numbers in color represent the dates of the two large dune erosion events (vertical dashed lines).

### 3.3.1. Hindcast

The hindcast results (covering the span of the data time series) for Profile 1 (Figure 9a) and Profile 3 (Figure 9c) show that the model is capable of reproducing the contour elevation changes, with  $R^2$  values ranging from 0.72 to 0.95. At Profile 1, the ShoreFor model performed poorly ( $R^2$  values ranging from 0.1 to 0.53) since it only captures the long-term trend, which is not directly related to the wave forcing. At Profile 3, the ShoreFor model performs better, especially in the upper and middle part of the beach, capturing some of the annual oscillations. However, similar to Profile 1, the model coefficients are primarily controlled by the long-term trend. This is more evident in the upper part of the beach for Profile 3 (Figure 9c, upper panel), where shoreline advance is observed between the two large dune erosion events, generating a large oscillation (38% of the E.V, Figure 8d, third panel) that is not captured by the ShoreFor model.

### 3.3.2. Forecast

A test of the model predictive skill was performed by training the model with 12 years of data, and then forecasting the remaining 2.5 years of shoreline evolution (gray area, Figure 9b and 9d). In general, the SPADS model showed good performance when predicting the last 2.5 years of shoreline changes (yellow lines), except for the lower part of the intertidal zone of Profile 3 (Figure 9d, lower panel), where the model underestimated the long-term trend while still following the annual cycle. The ShoreFor model behavior performed similarly (orange line) during the forecast and hindcast runs, except for lower part of the intertidal zone of Profile 1 (Figure 9b, lower panel) where, surprisingly, the model captured better the annual cycle and the long-term trend in comparison to the hindcast results (Figure 9a, lower panel).

## 4. Discussion

### 4.1. Beach Migration Modes

A centroid analysis was carried out considering both the dune and the intertidal beach volumes (scheme Figure 3b), allowing the identification of large changes in the dune-beach system. This study showed that despite the dominant beach sediment loss trend, the beach experienced different behavior in the upper and lower parts of the intertidal zone. During the study period, the beach profile experienced mainly steepening (advances in the upper intertidal zone, and retreat in the lower intertidal zone), in which the loss of sediment in the lower part of the beach was larger than the gain of sediment in the upper part (dune and berm recovery, Figure 7), indicating an overall decrease in sediment volume along the intertidal profile. Contour elevations along the upper part of the beach showed a long-term advance trend (Figures 8a and 8d, bottom panels), in agreement with the dominant steepening mode. The analysis also allowed identifying differences in beach translation/rotation modes. For instance, the flattening mode only generates changes in the steepening interval (cluster) when the dune face and the upper part of the beach are eroded, redistributing large amount of sediments along the lower intertidal beach due to storm events (Figures 3–5). Although the flattening mode was observed frequently (Figure 6), in general, this was caused by the lower part of the dune and berm being eroded, without a large amount of sediment being redistributed in the lower intertidal zone. In agreement with Townend and McLaren (1988) and Taylor et al. (2004), our analysis showed that the beach might experience steepening/flattening modes in addition to a net profile retreat or advance.

Different studies have addressed beach/dune sediment exchanges based on volume analyses with the goal of classifying the beach response during storm and recovery periods (Beuzen et al., 2019; Burvinct et al., 2017; Phillips et al., 2019; Taylor et al., 2004). Based on volumetric changes, Burvinct et al. (2017) used hierarchical clustering to analyze beach migration modes during extreme storms at 157 beaches in England. In contrast to the centroid analysis, the volume computations for the upper and lower parts of the beach require defining a pivot point (nodal point), which is not always evident and may even change in time, making the analysis difficult. Moreover, contributions of the dune system to the beach dynamics were neglected in their analysis. Phillips et al. (2019) used a decision tree classification and described four behavioral modes of subaerial profile variability during berm recovery. However, they also neglected the dune contributions in their study. Using a Bayesian network analysis, Beuzen et al. (2019) indicated that variability in berm and dune storm erosion was controlled by morphological conditions such as exposure to incident waves, pre-storm beach sand volume, and pre-storm beach width. Similar results were found in studies of the impact of the 2013/2014 winter storms on the UK coastline, where variability in coastal storm erosion response

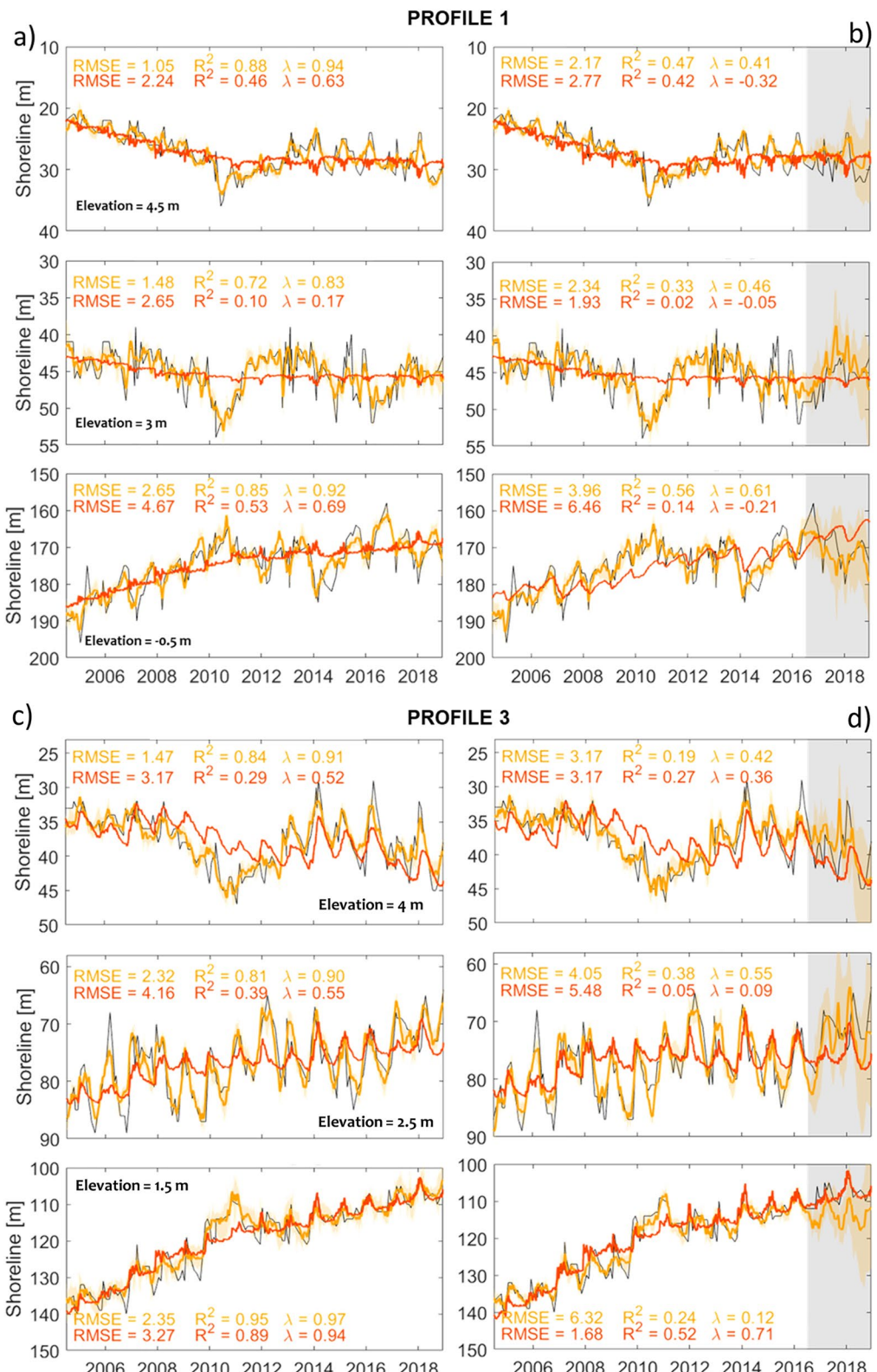


**Figure 9.** Model performance at three vertical elevations (same as shown in Figure 7) for Profile 1: (a) hindcast; (b) forecast; and Profile 3: (c) hindcast; (d) forecast, showing the shoreline measurements (black lines), the SPADS model (yellow lines and metrics), the ShoreFor Model (orange lines and metrics).

was attributed to the coastline indentation and the associated variability in beach orientation and direction of incident wave attack (Burvingt et al., 2018; Masselink, Scott, et al., 2016). In this study, in addition to the Curnic jetty influence, the differences in the beach/dune response between profiles 1 and 2 (behaving similarly) and Profile 3 may be attributed to the profile exposure to incoming waves. As can be seen in Figure 1b, local refraction and diffraction effects likely cause differences in the nearshore wave field, which may also explain the more evident annual volume changes observed at Profile 3 (Figure 6).

#### 4.2. Implications for Shoreline Modeling

In macro-tidal environments, the wave conditions, hydrodynamic processes, and duration of exposure to these conditions depend on the elevation in the intertidal zone (Masselink & Short, 1993). Equilibrium models have been tested previously at macro and meso-tidal beaches displaying different behavior across the intertidal zone (Castelle et al., 2014; Lemos et al., 2018). Sediment eroded from the upper intertidal zone is expected to be transported to the lower intertidal zone, much like the redistribution of sediment along the full profile of micro-tidal beaches (e.g., Winant et al., 1975; Yates et al., 2009). This study shows that when shoreline oscillations are analyzed in terms of their dominant time-scales, temporal oscillations in the upper (Figure 8a) and lower (Figure 8c) part of the beach are observed to be out of phase for Profile 1. This is in agreement with the predominant steepening/flattening processes observed for this profile. This was not as evident at intra-annual time-scales for Profile 3. Waves at Vougot Beach are characterized by a strong seasonal-annual signal (Figures 2g and 2h). Nonetheless, previous studies at Vougot Beach have found that there is no correlation between wave conditions and beach volume changes (Dodet et al., 2019). The authors argued that the beach–dune system continually lost sediment, independent of the wave conditions, due to the construction of the Curnic jetty preventing the sediment fluxes coming from the east (Suanez et al., 2010). Therefore, the long-term trend of chronic erosion is not directly related to wave forcing, but to sediment scarcity, and the longshore current dynamics. However, in the short term, a significant cross-correlation was observed between beach volume changes and extreme water levels (Suanez et al., 2015). However, Figure 6c shows that volume changes along Profile 3 display a strong annual cycle, and even profiles 1 and 2 also display a strong annual cycle after the highly energetic 2013/2014 winter. The analysis presented here also allowed identifying the different time-scales of shoreline changes and the drivers that dominate the observed changes, showing that the annual scale has an important role in explaining changes at certain cross-shore elevations (Figure 8). This could explain why the ShoreFor model had a better performance in the profiles where the annual scale was important.

Observations of large sediment exchanges between the beach and the dune showed that dune contributions play an important role in shoreline evolution. In particular, most beach-only shoreline change models predict shoreline retreat during large storm events, while the opposite may be true if dune erosion contributes sediment to the beach, causing shoreline advance. The developed method showed that some of the oscillations with higher explained variance than the annual time-scale were related to dune morphodynamics and accounted for both the erosion events and the subsequent dune recovery phase ( $T \sim 3,400$  days), which was associated with a period when no extreme storms and water levels occurred, allowing the upper beach and dune to recover. We notice that the oscillations at this time-scale are entirely dependent on the occurrence of major storms and likely vary for different sites based on the overall wave and/or atmospheric climate. This highlights the importance of linking dune and beach interactions to improve shoreline predictions. The relevance of this time-scale was different among the different profiles and contour elevations, in particular having a more important role along the upper part of the beach. Although the proposed modeling approach does not directly consider dune processes, it is able to reproduce shoreline changes related to dune sediment contributions. The model makes use of the SLP field and gradients, which contain information about the mean sea level fluctuations and large atmospheric patterns (Montaño et al., 2021; Camus, Menéndez, Méndez, Izaguirre, et al., 2004; Camus, Menéndez, Méndez, Losada, et al., 2004) such as the North Atlantic Oscillation index, which have been related to dune erosion/accretion events at Vougot (Suanez et al., 2015) and the West Europe Pressure Anomaly (Castelle et al., 2017) which have been found to control beach evolution in the latitudes of Brittany and southern England (Dodet et al., 2019; Scott et al., 2020). Therefore, including SPL fields and their gradient as drivers in the model becomes a surrogate for processes that cause dune erosion.

The majority of shoreline change models (excluding detailed process-based models such as XBeach) are not able to take into account the beach/dune sediment exchanges. For example, the ShoreFor model does not account for these interactions, so the observed poor skill on beach where interactions with dunes are important is not surprising. Interestingly, ShoreFor demonstrates better performance during the forecast period than when the whole dataset was used for calibration for Profile 1 (Figure 8b, bottom panel). The reduced skill during the hindcast is likely due to the shoreline being characterized by an E.V that is distributed similarly among the different IMFs (Figure 8c). Overall, ShoreFor tries to optimize a single parameter to account for all time-scales (and their interactions), whereas the newly proposed approach treats each time-scale separately and is hence able to reproduce better different physical processes acting on shorter and longer time-scales.

A variety of models have been proposed to predict dune and beach evolution, but only a limited number of them predict the effects of beach and dune interactions on multiple time-scales (Antolínez et al., 2019; Hanson et al., 2010; Larson et al., 2016; Palalane et al., 2016). One of the limitations of these models is that they are based on assuming a schematized profile shape, usually with a fixed berm, neglecting seasonal changes. In addition, in some of these models, sediments transported to the beach from dune erosion are redistributed throughout the whole profile instantaneously, neglecting lags in the distribution to the lower parts of the shoreface profile (Antolínez et al., 2019; Suárez et al., 2012). The analysis presented here indicates that the shoreline response due to sediment contributions from dunes is strongly dependent on the contour elevation (Figure 8), a feature that numerical models will need to address.

Another complication for modeling dune-beach interactions is that different drivers control both the spatial extent and temporal response of the beach (Morton et al., 1994; Phillips et al., 2019). The upper part of the beach is mainly controlled by wave action and the antecedent morphology (Davidson et al., 2013; Yates et al., 2009) while dune erosion has been found to be the combined result of wave action and TWLs (Kriebel & Dean, 1985; Larson et al., 2004; Vellinga, 1982). Furthermore, patterns of berm crest formation and vertical growth were found to be primarily governed by neap-spring tide variations in TWLs (Phillips et al., 2019). The current model suggests that the sediment contribution to shoreline changes due to dune erosion events (e.g.,  $T \sim 3,400$  days), which accounts for the 28% and 38% of the E.V in the upper part of the intertidal zone for profiles 1 and 3, are indirectly taken into account.

## 5. Conclusions

Almost 15 years of intertidal beach/dune profile measurements at Vougot Beach were analyzed to study the influence of the dune system on shoreline changes and the implications for shoreline modeling and prediction. Three different cross-shore profiles that display long-term erosion were first analyzed using a centroid analysis. The separation between the three identified clusters in the quadrant IV direction as a result of retreat was more evident for Profile 3. The centroid analysis also identified differences in the beach response for the upper and lower parts of the beach, showing long-term steepening trends (in the direction of quadrant I). Nonetheless, two large dune erosion events had significant impacts on each profile (migration from one cluster to the other) by flattening the beach, temporarily slowing down the retreat.

The CEEMD analysis allowed identifying the main time-scales of the observed shoreline changes, showing that a large percentage of the explained variance along the upper intertidal beach was related to time-scales associated with the two large dune erosion events and the subsequent recovery phases. In contrast, the lower part of the beach was dominated by a long-term erosion trend. For the profile least influenced by the jetty (Profile 3) the annual scale contributed significantly to the shoreline explained variance. However, the other two profiles (profiles 1 and 2) also showed an increase in the importance of the annual cycle signal after the 2013/2014 stormy winter, showing the importance of models that are able to capture the non-stationarity of shoreline evolution processes. These findings provide useful insight to understand that in addition to the expected seasonal-annual shoreline changes caused by incident wave variability or long-term changes associated with longshore sediment transport, other time-scales of changes may co-exist and have significant impacts on shoreline changes. As a result, this modeling approach was able to reproduce well shoreline changes at Vougot Beach, including interactions with the dunes, where traditional equilibrium models have displayed poor skill. By taking into account the dune-beach interaction, the model is able to reproduce the

time-scales related to the erosion and recovery of the dunes with a commensurate adjustment (e.g., rotation or translation) in the beach profile. The dune-beach interaction is critical for understanding the behavior of the beach system and the impact of the dunes on the shoreline position. We therefore contend that capturing the dominant time-scales in the forcing events and subsequent responses and mapping these using a centroid analysis provide sufficient insight to enable the observed changes to be satisfactorily explained. Overall, this methodology helps to improve understanding of beach-dune interactions, and even more generally, prediction horizons at beaches where a variety of processes operate, and traditional approaches fail.

## Data Availability Statement

Vougot profile data are available via the INDIGEO WEB platform (<https://commons.datacite.org/doi.org/10.35110/c120a3fe-9341-4bb3-b58b-1be6ba1deb99>). Suanez, Blaise, Cancouët, et al. (2016). Données pluri-décennales de suivi de profils de la plage/dune du Vougot à Guissény (Finistère, France). Roscoff tide gauge records are available at REFMAR-data-SHOM (<http://refmar.shom.fr/fr/donnees-refmar-sur-data.shom.fr/acces-aux-donnees>). Wave information used in this analysis can be obtained from HOMERE database (<http://doi.org/10.12770/cf47e08d-1455-4254-955e-d66225c9dc90>).

## Acknowledgments

This study was supported by ISblue project, Interdisciplinary graduate school for the blue planet (ANR-17-EURE-0015) and co-funded by a grant from the French government under the program "Investissements d'Avenir," which funded my research stay at the Laboratoire Géosciences Ocean (LGO UMR 6538 CNRS) – Université de Bretagne Occidentale, and the Laboratoire d'Hydraulique Saint-Venant (LHSV) – Université de Paris-Est. The survey of the Vougot beach is realized in the framework of the french "Service National d'Observation" (SNO) DY-NALIT labelled by the Institut National des Sciences de l'Univers (INSU) and co-funded by the CNRS (Centre National de la Recherche Scientifique).

## References

- Antolínez, J. A. A., Méndez, F. J., Anderson, D., Ruggiero, P., & Kaminsky, G. M. (2019). Predicting climate-driven coastlines with a simple and efficient multiscale model. *Journal of Geophysical Research: Earth Surface*, 124, 1596–1624. <https://doi.org/10.1029/2018JF004790>
- Ashton, A., Murray, A. B., & Arnault, O. (2001). Formation of coastline features by large-scale instabilities induced by high-angle waves. *Letters to Nature*, 414, 1–6. <https://doi.org/10.1038/35104541>
- Barnard, P. L., Short, A. D., Harley, M. D., Splinter, K. D., Vitousek, S., Turner, I. L., et al. (2015). Coastal vulnerability across the Pacific dominated by El Niño/Southern Oscillation. *Nature Geoscience*, 8(10), 801–807. <https://doi.org/10.1038/ngeo2539>
- Beuzen, T., Harley, M. D., Splinter, K. D., & Turner, I. L. (2019). Controls of variability in Berm and Dune storm erosion. *Journal of Geophysical Research: Earth Surface*, 124, 2647–2665. <https://doi.org/10.1029/2019JF005184>
- Blaise, E., Suanez, S., Stephan, P., Fichaut, B., David, L., Cuq, V., et al. (2015). Bilan des tempêtes de l'hiver 2013–2014 sur la dynamique de recul du trait de côte en Bretagne. *Géomorphologie: Relief, Processus, Environnement*, 21(3), 267–292. <https://doi.org/10.4000/géomorphologie.11104>
- Blossier, B., Bryan, K. R., Daly, C. J., & Winter, C. (2017). Shore and bar cross-shore migration, rotation and breathing processes at an embayed beach. *Journal of Geophysical Research: Earth Surface*, 122, 1745–1770. <https://doi.org/10.1002/2017JF004227>
- Boak, E. H., & Turner, I. L. (2005). Shoreline definition and detection: A review. *Journal of Coastal Research*, 214(214), 688–703. <https://doi.org/10.2112/03-0071.1>
- Boudière, E., Maisondieu, C., Ardhuin, F., Accensi, M., Pineau-Guilhou, L., & Lepesqueur, J. (2013). A suitable metocean hindcast database for the design of Marine energy converters. *International Journal of Marine Energy*, 3(4), 40–e52. <https://doi.org/10.1016/j.ijome.2013.11.010>
- Bruun, P. (1962). Sea-level rise as a cause of shore erosion. *Journal of the Waterways and Harbors Division*, 88(1), 117–130. <https://doi.org/10.1061/jwheaw.0000252>
- Bruun, P. (1988). The Bruun Rule of Erosion by sea-level rise: A discussion on large-scale two- and three-dimensional. *Journal of Coastal Research*, 4(4), 627–648.
- Burvingt, O., Masselink, G., Russell, P., & Scott, T. (2017). Classification of beach response to extreme storms. *Geomorphology*, 295, 722–737. <https://doi.org/10.1016/j.geomorph.2017.07.022>
- Burvingt, O., Masselink, G., Scott, T., Davidson, M., & Russell, P. (2018). Climate forcing of regionally-coherent extreme storm impact and recovery on embayed beaches. *Marine Geology*, 401, 112–128. <https://doi.org/10.1016/j.margeo.2018.04.004>
- Callaghan, D. P., Nielsen, P., Short, A., & Ranasinghe, R. (2008). Statistical simulation of wave climate and extreme beach erosion. *Coastal Engineering*, 55(5), 375–390. <https://doi.org/10.1016/j.coastaleng.2007.12.003>
- Camus, P., Menendez, M., Mendez, F. J., Izaguirre, C., Espejo, A., Canovas, V., et al. (2014a). A weather-type statistical downscaling framework for ocean wave climate. *Journal of Geophysical Research: Oceans*, 119, 3909–3925. <https://doi.org/10.1002/2013JC009563>
- Camus, P., Menéndez, M., Méndez, F. J., Losada, I. J., Espejo, A., Pérez, J., et al. (2014b). A method for finding the optimal predictor indices for local wave climate conditions. *Ocean Dynamics*, 64(7), 1025–1038. <https://doi.org/10.1007/s10236-014-0737-2>
- Cariolet, J. M., & Suanez, S. (2013). Runup estimations on a macrotidal sandy beach. *Coastal Engineering*, 74, 11–18. <https://doi.org/10.1016/j.coastaleng.2012.11.008>
- Castelle, B., Dodet, G., Masselink, G., & Scott, T. (2017). A new climate index controlling winter wave activity along the Atlantic coast of Europe: The West Europe Pressure Anomaly. *Geophysical Research Letters*, 44(3), 1384–1392. <https://doi.org/10.1029/2016GL072379>
- Castelle, B., Marieu, V., Bujan, S., Ferreira, S., Paridot, J. P., Capo, S., et al. (2014). Equilibrium shoreline modelling of a high-energy meso-macrotidal multiple-barred beach. *Marine Geology*, 347, 85–94. <https://doi.org/10.1016/j.margeo.2013.11.003>
- Castelle, B., Marieu, V., Bujan, S., Splinter, K. D., Robinet, A., Sénéchal, N., & Ferreira, S. (2015). Impact of the winter 2013–2014 series of severe Western Europe storms on a double-barred sandy coast: Beach and dune erosion and megacusp embayments. *Geomorphology*, 238, 135–148. <https://doi.org/10.1016/j.geomorph.2015.03.006>
- Castelle, B., Ruessink, B. G., Bonneton, P., Marieu, V., Bruneau, N., & Price, T. D. (2010). Coupling mechanisms in double sandbar systems. Part 1: Patterns and physical explanation. *Earth Surface Processes and Landforms*, 486, 476. <https://doi.org/10.1002/esp.1929>
- Coco, G., Senechal, N., Rejas, A., Bryan, K. R., Capo, S., Paridot, J. P., et al. (2014). Beach response to a sequence of extreme storms. *Geomorphology*, 204, 493–501. <https://doi.org/10.1016/j.geomorph.2013.08.028>
- Cohn, N., Ruggiero, P., de Vries, S., & Kaminsky, G. M. (2018). New insights on Coastal foredune growth: The relative contributions of Marine and Aeolian processes. *Geophysical Research Letters*, 45(10), 4965–4973. <https://doi.org/10.1029/2018GL077836>

- Conlin, M. P., Adams, P. N., Jaeger, J. M., & MacKenzie, R. (2020). Quantifying seasonal-to-interannual-scale storm impacts on morphology along a Cuspate Coast with a hybrid empirical orthogonal function approach. *Journal of Geophysical Research: Earth Surface*, 125(12). <https://doi.org/10.1029/2020JF005617>
- D'Anna, M., Idier, D., Castelle, B., Cozannet, G. L., Rohmer, J., & Robinet, A. (2020). Impact of model free parameters and sea-level rise uncertainties on 20-years shoreline hindcast: The case of Truc Vert beach (SW France). *Earth Surface Processes and Landforms*, 45, 1895–1907. <https://doi.org/10.1002/esp.4854>
- Davidson, M. A., Splinter, K. D., & Turner, I. L. (2013). A simple equilibrium model for predicting shoreline change. *Coastal Engineering*, 73, 191–202. <https://doi.org/10.1016/j.coastaleng.2012.11.002>
- Dissanayake, P., Brown, J., Wisse, P., & Karunarathna, H. (2015). Effects of storm clustering on beach/dune evolution. *Marine Geology*, 370, 63–75. <https://doi.org/10.1016/j.margeo.2015.10.010>
- Dodet, G., Castelle, B., Masselink, G., Scott, T., Davidson, M., Floc'h, F., et al. (2019). Beach recovery from extreme storm activity during the 2013–14 winter along the Atlantic coast of Europe. *Earth Surface Processes and Landforms*, 44(1), 393–401. <https://doi.org/10.1002/esp.4500>
- Duveiller, G., Fasbender, D., & Meroni, M. (2016). Revisiting the concept of a symmetric index of agreement for continuous datasets. *Scientific Reports*, 6, 1–14. <https://doi.org/10.1038/srep19401>
- Hanson, H. (1989). Genesis—A generalized shoreline change numerical model. *Journal of Coastal Research*, 5(1), 1–27.
- Hanson, H., Larson, M., & Kraus, N. C. (2010). Calculation of beach change under interacting cross-shore and longshore processes. *Coastal Engineering*, 57(6), 610–619. <https://doi.org/10.1016/j.coastaleng.2010.02.002>
- Hapke, C. J., Plant, N. G., Henderson, R. E., Schwab, W. C., & Nelson, T. R. (2016). Decoupling processes and scales of shoreline morphodynamics. *Marine Geology*, 381, 42–53. <https://doi.org/10.1016/j.margeo.2016.08.008>
- Hegermiller, C. A., Antolinez, J. A. A., Rueda, A., Camus, P., Perez, J., Erikson, L. H., et al. (2017). A multimodal wave spectrum-based approach for statistical downscaling of local wave climate. *Journal of Physical Oceanography*, 47(2), 375–386. <https://doi.org/10.1175/JPO-D-16-0191.1>
- Houser, C. (2009). Synchronization of transport and supply in beach-dune interaction. *Progress in Physical Geography*, 33(6), 733–746. <https://doi.org/10.1177/0309133093051020>
- Huang, N. E., Shen, Z., Long, S. R., Wu, M. C., Shih, H. H., Zheng, Q., et al. (1998). The empirical mode decomposition and the Hilbert spectrum for nonlinear and non-stationary time series analysis. *Proceedings of the Royal Society A: Mathematical, Physical & Engineering Sciences*, 454, 903–995. <https://doi.org/10.1098/rspa.1998.0193>
- Hurst, M. D., Barkwith, A., Ellis, M. A., Thomas, C. W., & Murray, A. B. (2015). Exploring the sensitivities of crenulate bay shorelines to wave climates using a new vector-based one-line model. *Journal of Geophysical Research: Earth Surface*, 120(12), 2586–2608. <https://doi.org/10.1002/2015JF003704>
- Kriebel, D., & Dean, R. G. (1985). Numerical simulation of time-dependent beach and dune erosion. *Coastal Engineering*, 9, 221–245. [https://doi.org/10.1016/0378-3839\(85\)90009-2](https://doi.org/10.1016/0378-3839(85)90009-2)
- Larson, M., Erikson, L., & Hanson, H. (2004). An analytical model to predict dune erosion due to wave impact. *Coastal Engineering*, 51(8–9), 675–696. <https://doi.org/10.1016/j.coastaleng.2004.07.003>
- Larson, M., & Kraus, N. C. (1995). Prediction of cross-shore sediment transport at different spatial and temporal scales. *Marine Geology*, 126(1–4), 111–127. [https://doi.org/10.1016/0025-3227\(95\)00068-A](https://doi.org/10.1016/0025-3227(95)00068-A)
- Larson, M., Palalane, J., Fredriksson, C., & Hanson, H. (2016). Simulating cross-shore material exchange at decadal scale. Theory and model component validation. *Coastal Engineering*, 116, 57–66. <https://doi.org/10.1016/j.coastaleng.2016.05.009>
- Le Cozannet, G., Bulteau, T., Castelle, B., Ranasinghe, R., Wöppelmann, G., Rohmer, J., et al. (2019). Quantifying uncertainties of sandy shoreline change projections as sea level rises. *Scientific Reports*, 9(1), 1–11. <https://doi.org/10.1038/s41598-018-37017-4>
- Lemos, C., Floc'h, F., Yates, M., Le Dantec, N., Marieu, V., Hamon, K., et al. (2018). Equilibrium modeling of the beach profile on a macrotidal embayed low tide terrace beach. *Ocean Dynamics*, 68(9), 1207–1220. <https://doi.org/10.1007/s10236-018-1185-1>
- Ludka, B. C., Guza, R. T., O'Reilly, W. C., Merrifield, M. A., Flick, R. E., Bak, A. S., et al. (2019). Sixteen years of bathymetry and waves at San Diego beaches. *Scientific Data*, 6(1), 161. <https://doi.org/10.1038/s41597-019-0167-6>
- Luijendijk, A., Hagenaars, G., Ranasinghe, R., Baart, F., Donchyts, G., & Aarninkhof, S. (2018). The state of the world's beaches. *Scientific Reports*, 8(1), 6641. <https://doi.org/10.1038/s41598-018-24630-6>
- Masselink, G., Castelle, B., Scott, T., Dodet, G., Suanez, S., Jackson, D., & Floc'h, F. (2016a). Extreme wave activity during 2013/2014 winter and morphological impacts along the Atlantic coast of Europe. *Geophysical Research Letters*, 43, 2135–2143. <https://doi.org/10.1002/2015GL067492.Received>
- Masselink, G., Scott, T., Poate, T., Russell, P., Davidson, M., & Conley, D. (2016b). The extreme 2013/2014 winter storms: Hydrodynamic forcing and coastal response along the southwest coast of England. *Earth Surface Processes and Landforms*, 41(3), 378–391. <https://doi.org/10.1002/esp.3836>
- Masselink, G., & Short, A. D. (1993). The effect of tide range on beach morphodynamics and morphology: A conceptual beach model. *Journal of Coastal Research*, 9(3), 785–800.
- Matthews, T., Murphy, C., Wilby, R. L., & Harrigan, S. (2014). Stormiest winter on record for Ireland and UK. *Nature Climate Change*, 4(9), 738–740. <https://doi.org/10.1038/nclimate2336>
- Miller, J. K., & Dean, R. G. (2004). A simple new shoreline change model. *Coastal Engineering*, 51, 531–556. <https://doi.org/10.1016/j.coastaleng.2004.05.006>
- Montaña, J., Blossier, B., Osorio, A. F., & Winter, C. (2020). The role of frequency spread on swash dynamics. *Geo-Marine Letters*, 40, 243–254. <https://doi.org/10.1007/s00367-019-00591-1>
- Montaña, J., Coco, G., Antolinez, J. A. A., Beuzen, T., Bryan, K. R., Cagigal, L., et al. (2020). Blind testing of shoreline evolution models. *Scientific Reports*, 10(1), 1–10. <https://doi.org/10.1038/s41598-020-59018-y>
- Montaña, J., Coco, G., Cagigal, L., Mendez, F., Rueda, A., Bryan, K. R., & Harley, M. D. (2021). A multiscale approach to shoreline prediction. *Geophysical Research Letters*, 48(1), 1–11. <https://doi.org/10.1029/2020gl090587>
- Morton, R. A., Paine, J. G., & Gibeaut, J. C. (1994). Stages and durations of post-storm beach recovery, Southeastern Texas Coast, U.S. *Journal of Coastal Research*, 10(4), 884–908.
- Nicholls, R. J., & Cazenave, A. (2010). Sea level rise and its impact on coastal zones. *Science*, 328, 1517–1520. <https://doi.org/10.1126/science.1185782>
- Palalane, J., Fredriksson, C., Marinho, B., Larson, M., Hanson, H., & Coelho, C. (2016). Simulating cross-shore material exchange at decadal scale. Model application. *Coastal Engineering*, 116, 26–41. <https://doi.org/10.1016/j.coastaleng.2016.05.007>

- Pérez, J., Méndez, F. J., Menéndez, M., & Losada, I. J. (2014). ESTELA: A method for evaluating the source and travel time of the wave energy reaching a local area. *Ocean Dynamics*, 64, 1181–1191. <https://doi.org/10.1007/s10236-014-0740-7>
- Pérez-Alberti, A., & Trenhaile, A. S. (2015). Clast mobility within boulder beaches over two winters in Galicia, northwestern Spain. *Geomorphology*, 248, 411–426. <https://doi.org/10.1016/j.geomorph.2015.08.001>
- Phillips, M. S., Blenkinsopp, C. E., Splinter, K. D., Harley, M. D., & Turner, I. L. (2019). Modes of Berm and Beach face recovery following storm reset: Observations using a continuously scanning Lidar. *Journal of Geophysical Research: Earth Surface*, 124(3), 720–736. <https://doi.org/10.1029/2018JF004895>
- Phillips, M. S., Harley, M. D., Turner, I. L., Splinter, K. D., & Cox, R. J. (2017). Shoreline recovery on wave-dominated sandy coastlines: The role of sandbar morphodynamics and nearshore wave parameters. *Marine Geology*, 385, 146–159. <https://doi.org/10.1016/j.margeo.2017.01.005>
- Plant, N. G., & Stockdon, H. F. (2012). Probabilistic prediction of barrier-island response to hurricanes. *Journal of Geophysical Research: Earth Surface*, 117(3), 1–n. <https://doi.org/10.1029/2011JF002326>
- Rasche, N., & Arduin, F. (2013). A global wave parameter database for geophysical applications. Part 2: Model validation with improved source term parameterization. *Ocean Modelling*, 70, 174–188. <https://doi.org/10.1016/j.ocemod.2012.12.001>
- Robinet, A., Idier, D., Castelle, B., & Marieu, V. (2018). A reduced-complexity shoreline change model combining longshore and cross-shore processes: The LX-Shore model. *Environmental Modelling & Software*, 109, 1–16. <https://doi.org/10.1016/j.envsoft.2018.08.010>
- Rueda, A., Cagigal, L., Antolinez, J. A. A., Albuquerque, J. C., Castanedo, S., Coco, G., & Méndez, F. J. (2019). Marine climate variability based on weather patterns for a complicated island setting: The New Zealand case. *International Journal of Climatology*, 39(3), 1777–1786. <https://doi.org/10.1002/joc.5912>
- Ruggiero, P., Komar, P. D., McDougal, W. G., Marra, J. J., & Beach, R. A. (2001). Wave runup, extreme water levels and the erosion of properties backing beaches. *Journal of Coastal Research*, 17(2), 407–419.
- Scott, T., Masselink, G., McCarroll, R. J., Russell, P., & Russell, P. (2020). Predicting beach rotation using multiple atmospheric indices. *Marine Geology*, 426, 106207. <https://doi.org/10.1016/j.margeo.2020.106207>
- Senechal, N., Coco, G., Castelle, B., & Marieu, V. (2015). Storm impact on the seasonal shoreline dynamics of a meso- to macrotidal open sandy beach (Biscarrosse, France). *Geomorphology*, 228, 448–461. <https://doi.org/10.1016/j.geomorph.2014.09.025>
- Serafin, K. A., & Ruggiero, P. (2014). Simulating extreme total water levels using a time-dependent, extreme value approach. *Journal of Geophysical Research: Oceans*, 119, 6305–6329. <https://doi.org/10.1002/2014JC010093.Received>
- Soulsby, R., Sutherland, J., & Brampton, A. (1999). Coastal steepening - the UK view. (HR Wallingford Technical Report: TR91). <https://eprints.hrwallingford.com/437/1/TR91.pdf>
- Splinter, K. D., & Palmsten, M. L. (2012). Modeling dune response to an East Coast Low. *Marine Geology*, 329–331, 46–57. <https://doi.org/10.1016/j.margeo.2012.09.005>
- Splinter, K. D., Turner, I. L., & Davidson, M. A. (2013). How much data is enough? The importance of morphological sampling interval and duration for calibration of empirical shoreline models. *Coastal Engineering*, 77, 14–27. <https://doi.org/10.1016/j.coastaleng.2013.02.009>
- Splinter, K. D., Turner, I. L., Davidson, M. A., Barnard, P., Castelle, B., & Oltman-Shay, J. (2014). A generalized equilibrium model for predicting daily to interannual shoreline response. *Journal of Geophysical Research: Earth Surface*, 119(9), 1936–1958. <https://doi.org/10.1002/2014JF003106>
- Suanez, S., Blaise, E., Cancouët, R., & Floc'h, F. (2016b). Empirical parameterization of wave runup and dune erosion during storm conditions on a natural macrotidal beach. *Journal of Coastal Research*, 75(sp1), 932–936. <https://doi.org/10.2112/si75-187.1>
- Suanez, S., Blaise, E., Cariot, J. M., & David, L. (2016a). Données pluri-décennales de suivi de profils de la plage/dune du Vougot à Guissény (Finistère, France).
- Suanez, S., Cancouët, R., Floc'h, F., Blaise, E., Ardhuin, F., Filipot, J.-F., et al. (2015). Observations and predictions of wave runup, extreme water levels, and medium-term dune erosion during storm conditions. *Journal of Marine Science and Engineering*, 3(3), 674–698. <https://doi.org/10.3390/jmse3030674>
- Suanez, S., Cariot, J., Cancouët, R., Ardhuin, F., & Delacourt, C. (2012). Dune recovery after storm erosion on a high-energy beach: Vougot Beach, Brittany (France). *Geomorphology*, 139–140, 16–33. <https://doi.org/10.1016/j.geomorph.2011.10.014>
- Suanez, S., Cariot, J., & Fichaut, B. (2010). Monitoring of recent morphological changes of the dune. *Shore and Beach*, 78, 37–47.
- Suanez, S., & Cariot, J.-M. (2010). L'action des tempêtes sur l'érosion des dunes: Les enseignements de la tempête du 10 mars 2008Impact of storms on dune erosion: Lessons from the 10th March 2008 storm. *Norois*, (215), 77–99. <https://doi.org/10.4000/norois.3212>
- Taylor, J. A., Murdock, A. P., & Pontee, N. I. (2004). A macroscale analysis of coastal steepening around the coast of England and Wales. *Geographical Journal*, 170(3), 179–188. <https://doi.org/10.1111/j.0016-7398.2004.00119.x>
- Torres, M., Colominas, M. A., Schlotthauer, G., & Flandrin, P. (2011). A complete ensemble empirical mode decomposition with adaptive noise. In *Paper presented at the IEEE International Conference on Acoustics, Speech and Signal Processing (ICASSP)* (pp. 4144–4147). Retrieved from [http://ieeexplore.ieee.org/xpls/abs\\_all.jsp?arnumber=5947265](http://ieeexplore.ieee.org/xpls/abs_all.jsp?arnumber=5947265)
- Townend, I. H. (2018). *Coastal tools manual*. [www.coastalsea.uk](http://www.coastalsea.uk)
- Townend, I. H., Fleming, C. A., McLaren, P., & Hunter-Blair, A. (1990). A regional study of coastal morphology. *Paper presented at the International Conference of Coastal Engineering* (pp. 2589–2602). American Society of Civil Engineers. <https://doi.org/10.9753/icce.v22.%p>
- Townend, I. H., & McLaren, P. (1988). *Anglian coastal management atlas*. *The Anglian Sea Defence Management Study-Stage II* (pp. 1–107). Sir William Halcrow and Partners report for Anglian Water.
- Turner, I. L., Harley, M. D., Short, A. D., Simmons, J. A., Bracs, M. A., Phillips, M. S., & Splinter, K. D. (2016). A multi-decade dataset of monthly beach profile surveys and inshore wave forcing at Narrabeen, Australia. *Scientific Data*, 3, 160024. <https://doi.org/10.1038/sdata.2016.24>
- US Army Corps of Engineers. (1984). *Shore protection manual*. <https://usace.contentdm.oclc.org/digital/collection/p16021coll11/id/1934/>
- Vellinga, P. (1982). Beach and dune erosion during storm surges. *Coastal Engineering*, 6, 361–387. [https://doi.org/10.1016/0378-3839\(82\)90007-2](https://doi.org/10.1016/0378-3839(82)90007-2)
- Villamarín, B. C. (2017). *Beach cross-shore dynamics: Applicability of equilibrium shoreline models*. University of Southampton.
- Vitousek, S., Barnard, P. L., Limber, P., Erikson, L., & Cole, B. (2017). A model integrating longshore and cross-shore processes for predicting long-term shoreline response to climate change. *Journal of Geophysical Research: Earth Surface*, 1, 782–806. <https://doi.org/10.1002/2016JF004065>
- Vos, K., Harley, M. D., Splinter, K. D., Simmons, J. A., & Turner, I. L. (2019). Sub-annual to multi-decadal shoreline variability from publicly available satellite imagery. *Coastal Engineering*, 150, 160–174. <https://doi.org/10.1016/j.coastaleng.2019.04.004>
- Wiggins, M., Scott, T., Masselink, G., McCarroll, R. J., & Russell, P. (2020). Predicting beach rotation using multiple atmospheric indices. *Marine Geology*, 426, 106207. <https://doi.org/10.1016/j.margeo.2020.106207>

- Winant, C. D., Inman, D. L., & Nordstrom, C. E. (1975). Description of seasonal beach changes using Empirical Eigenfunctions. *Journal of Geophysical Research*, 80(15), 1979–1986. <https://doi.org/10.1029/jc080i015p01979>
- Wright, L. D., Short, A. D., & Green, M. O. (1985). Short-term changes in the morphodynamic states of beaches and surf zones: An empirical predictive model. *Marine Geology*, 62(3–4), 339–364. [https://doi.org/10.1016/0025-3227\(85\)90123-9](https://doi.org/10.1016/0025-3227(85)90123-9)
- Wu, Z., & Huang, N. E. (2004). A study of the characteristics of white noise using the empirical mode decomposition method. *Proceedings of the Royal Society A: Mathematical, Physical and Engineering Sciences*, 460(2046), 1597–1611. <https://doi.org/10.1098/rspa.2003.1221>
- Yates, M. L., Guza, R. T., & Reilly, W. C. O. (2009). Equilibrium shoreline response: Observations and modeling. *Journal of Geophysical Research*, 114, 1–16. <https://doi.org/10.1029/2009JC005359>